Title: Conditional depletion reveals temporal requirements for the oscillating transcription factor NHR-23/NR1F1 in *C. elegans* larval progression

Londen C. Johnson[1], Joseph Aguilera[1], Max T. Levenson[1], Andreas Rechtsteiner[1], An A. Vo[1], J. Matt Ragle[1], and Jordan D. Ward[1‡].

[1]Department of Molecular, Cell, and Developmental Biology, University of California-Santa Cruz, Santa Cruz, CA 95064, USA.

[‡]Author for correspondence.

Corresponding author email: jward2@ucsc.edu

Keywords: *C. elegans*, molting, NHR-23, nuclear hormone receptor, apical extracellular matrix, auxin-inducible degron

Running Title: NHR-23 and larval progression

18 **Summary Statement**

19 This work provides insight into how a recently discovered large-scale gene expression
20 oscillator promotes rhythmic skin regeneration in *C. elegans.*

21

22

Abstract

Nematode molting is a remarkable process where the animals must essentially build a new epidermis underneath the old skin and then rapidly shed the old skin. The study of molting provides a gateway into the developmental program of many core cellular and physiological processes, such as oscillatory gene expression, coordinated intracellular trafficking, steroid hormone signaling, developmental timing, and extracellular remodeling. The nuclear hormone receptor NHR-23/NR1F1 is an important regulator of molting. Imaging and western blot time-courses revealed oscillatory NHR-23::GFP expression in the epithelium that closely followed the reported mRNA expression. Timed depletion experiments using the auxin-inducible degron system revealed that NHR-23/NR1F1 depletion early in a given larval stage caused animals to arrest with only weak molting defects, whereas later depletion resulted in highly penetrant severe molting and morphological defects. This larval arrest was independent of insulin signaling. Despite the weakly penetrant molting defects following early NHR-23/NR1F1 depletion, the epidermal barrier was defective suggesting that NHR-23/NR1F1 is necessary for establishing or maintaining this barrier. NHR-23/NR1F1 coordinates the expression of factors involved in molting, lipid transport/metabolism, and remodeling of the apical extracellular matrix. We propose that NHR-23/NR1F1 is a regulator in a recently discovered large-scale gene oscillatory network coordinating rhythmic skin regeneration.

Introduction

Molting is a critical developmental process required for the growth of all ecdysozoans, a clade comprising an estimated total of 4.5 million living species (Telford et al., 2008). Although specific to invertebrates, molting involves conserved processes such as apical extracellular matrix (aECM) remodeling, intracellular trafficking, and oscillatory gene expression (Lažetić and Fay, 2017). Molting is also a process of interest for developing new drugs against parasitic nematodes (Ghedin et al., 2007). This group of pathogens infect over one billion humans and devastate crops and livestock, yet few drugs exist to counter them and resistance is emerging (Ward, 2015b). While many genes involved in

54 nematode molting have been identified in *C. elegans* (Frand et al., 2005), little is known
55 about how their gene products are coordinated to promote aECM remodeling and the
56 generation and release of a new cuticle.
57
58 Nematodes progress through four periodic larval stages (L1-L4), prior to becoming a
59 reproductive adult (Brenner, 1974). The end of each larval stage is punctuated by a molt
60 that involves trafficking and secretion of aECM components, assembly of a new aECM
61 underneath the old cuticle, followed by separation of the cuticle from the underlying aECM
62 (apolysis) and shedding of the old cuticle (ecdysis)(Lažetić and Fay, 2017). Apolysis
63 coincides with a sleep-like behavior called lethargus (Singh and Sulston, 1978). The
64 cuticle is a collagenous exoskeleton secreted by hypodermal and seam epithelial cells
65 (Page and Johnstone, 2007). The outermost layer (glycocalyx) is rich in carbohydrates
66 and mucins and thought to be secreted by the excretory gland cell (Nelson et al., 1983;
67 Singh and Sulston, 1978). Beneath the glycocalyx is the glycolipid- and lipid-rich
68 epicuticle which is postulated to function as a hydrophobic surface barrier (Blaxter, 1993;
69 Blaxter et al., 1992). The composition and biogenesis of the glycocalyx and epicuticle are
70 poorly understood in comparison to the underlying layers composed of collagens and
71 cuticlins.
72
73 Nuclear hormone receptor (NHR) transcription factors are key regulators of molting in
74 insects and nematodes (King-Jones and Thummel, 2005; Taubert et al., 2011). NHRs are
75 characterized by a ligand-binding domain (LBD) which has the potential to bind small
76 molecules such as ligands and dietary-derived metabolites (Taubert et al., 2011). Not all
77 NHRs have known ligands, though the ancestral proteins from which all NHRs descend
78 bound ligands (Bridgham et al., 2010; Eick and Thornton, 2011). NHRs have a canonical
79 zinc finger DNA-binding domain (DBD) with an unstructured hinge region between the
80 DBD and LBD that is subject to post-translational regulation (Antebi, 2015; Campbell et
81 al., 2008; Ward et al., 2013). NHRs can function as homodimers, heterodimers, or
82 monomers (Sever and Glass, 2013).
83

There has been a large expansion of NHRs within nematode genomes, making direct comparisons to other organisms challenging (Antebi, 2015; Taubert et al., 2011). However, a single, conserved nuclear hormone receptor, NHR-23/NR1F1 (hereafter referred to as NHR-23), an ortholog of DHR3 in insects and RORalpha in mammals, is a key regulator of C. elegans molting. *nhr-23* mutation or inactivation by RNAi leads to embryonic lethality, larval arrest, ecdysis defects, and morphology defects (Frand et al., 2005; Gissendanner et al., 2004; Kostrouchova et al., 1998; Kostrouchova et al., 2001). *nhr-23* mRNA expression oscillates over the course of each larval stage, peaking mid-larval stage and hitting a trough at the molt (Gissendanner et al., 2004; Kostrouchova et al., 2001). Experiments with *nhr-23* mutants and RNAi have demonstrated a role for NHR-23 in all four larval molts (Kostrouchova et al., 1998; Kostrouchova et al., 2001), but these approaches didn't determine when during a given larval stage NHR-23 was necessary. Molting must be coordinated with developmental timing, though the underlying mechanisms linking these two are poorly understood. Uncoupling of the molting and heterochronic pathway through exposure to a nicotinic agonist causes death as animals attempt to molt without completing the requisite cell divisions and differentiation (Ruaud and Bessereau, 2006). Bacterial diet can alter developmental rate in *C. elegans*, likely through modification of NHR-23 activity (Macneil et al., 2013). The NHR-23 insect ortholog (DHR3) is part of the molting gene regulatory network (Lam et al., 1997; Ruaud et al., 2010, 3) and the mammalian ortholog (RORα) regulates circadian rhythms, lipid metabolism, and immunity (Jetten, 2009).

We found that NHR-23 protein oscillates and three distinct isoforms are expressed. Using the auxin-inducible degron system for rapid inactivation of NHR-23 during development, we discovered distinct phenotypes when NHR-23 was depleted early or late in a given larval stage. Early depletion leads to a larval arrest with mild molting defects, while later depletion resulted in penetrant molting and morphological defects. Analysis of NHR-23 target genes suggests a role in coordinating aECM assembly, remodeling, and construction of specific cuticular structures. Our work provides an entry point into understanding how NHR-23 coordinates the complex cell biology underpinning molting.

Results

NHR-23 protein oscillates during development

Expression of *nhr-23* mRNA oscillates throughout each larval stage of the *C. elegans* life cycle (Gissendanner et al., 2004; Hendriks et al., 2014; Kostrouchova et al., 2001; Meeuse et al., 2020) reaching peak expression mid-intermolt and a trough prior to the completion of the next molt (Fig. 1A). However, mRNA expression profiles do not always match protein levels (de Sousa Abreu et al., 2009; Vogel and Marcotte, 2012). For example, *C. elegans daf-12* mRNA transcripts oscillate during each larval stage, but the protein products are constitutively expressed (Antebi, 2015). To determine whether NHR-23 protein oscillates, we monitored the expression of the endogenous protein, tagged with green fluorescent protein (GFP), over the course of 28 hours. During L1, oscillating expression of NHR-23::GFP was observed in the nuclei of seam and hypodermal cells (Fig. S1). Expression of NHR-23 rises and falls prior to the completion of the 1st molt; this pattern is repeated prior to the 2nd molt as well (Fig. 1B,C), similar to the reported mRNA expression (Gissendanner et al., 2004; Kostrouchova et al., 2001).

As GFP tags can affect the expression or stability of proteins (Agbulut et al., 2006; Baens et al., 2006), we assayed the expression of NHR-23 through western blotting time-courses using an *nhr-23::AID*::3xFLAG* strain (Zhang et al., 2015). These experiments confirmed that NHR-23::AID*::3xFLAG also oscillates (Fig. 1C), similar to our NHR-23::GFP imaging experiments (Fig. 1B). We detected three distinct NHR-23 bands, consistent with the predicted sizes of *nhr-23b/f, nhr-23c,* and *nhr-23e* (Fig. 1C,D, Fig. S2). However, these bands could also reflect post-translational modification. All observed NHR-23 bands oscillate, though the lowest band was expressed more strongly than the other bands (Fig. 1C).

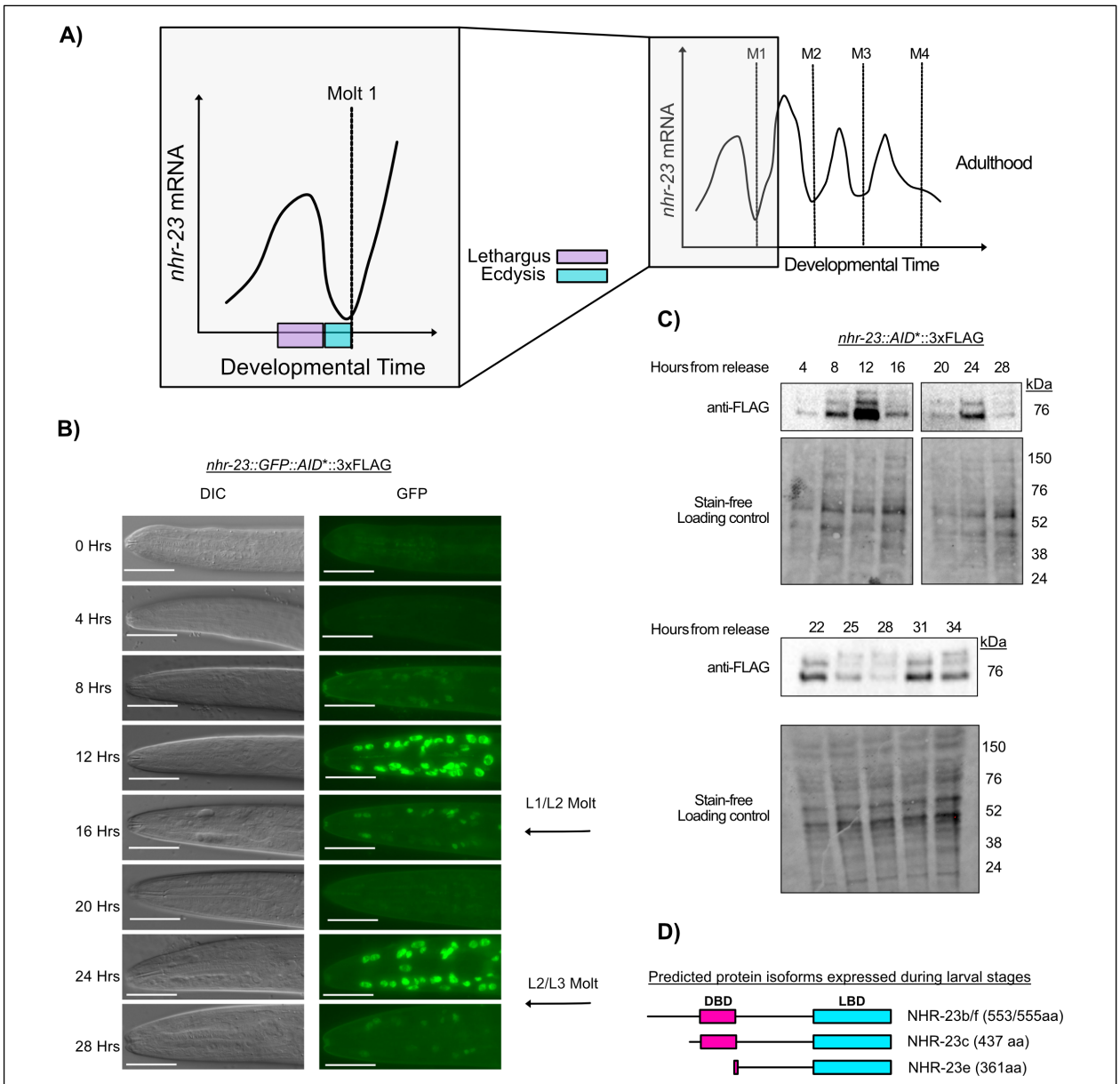

Figure 1: NHR-23 protein oscillates during development. (A) A schematic of *nhr-23* mRNA expression across *C.* elegans larval development created with BioRender.com. The relative abundance of mRNA is based on the qRT-PCR analysis by Gissendanner et al., 2004. (B) Representative images from a time course monitoring the expression of endogenous NHR-23 protein over the first 28 hours of larval development. The appropriate timing of the L1/L2 and L2/L3 molts is indicated. *nhr-23::GFP::AID*::3xFLAG* (B) and *nhr-23::AID*::3xFLAG* (C) are previously described endogenous knock-ins that produce C-terminal translational fusions to all known *nhr-23* isoforms (Ragle et al., 2020; Zhang et al., 2015). (C) Anti-FLAG immunoblot analysis of synchronized *nhr-23::AID**::3xFLAG animals monitoring the expression of NHR-23 3XFLAG across two time courses, 4-28 hours and 22-34 hours. Marker size (in kDa) is provided. Stain-free analysis, which visualizes total protein on the membrane, is provided as a loading control. (D) Cartoons of predicted protein isoforms expressed during larval development based on Nanopore direct mRNA sequencing data (Roach et al., 2020). All of the predicted isoforms contain a Ligand Binding Domain (LBD) while only two of the three have a DNA Binding Domain (DBD). The predicted size of each isoform is listed to the right of the structure in amino acids (aa).

142 *Distinct phenotypes are observed when NHR-23 is depleted early or late in L1 larvae*
143 Given that NHR-23 isoforms oscillate, we tested when NHR-23 was necessary for molting
144 during the L1 larval stage. We have previously shown that the auxin-inducible degron
145 system can rapidly deplete a nuclear hormone receptor (NHR-25), with almost complete
146 depletion within 30 minutes (Zhang et al., 2015). In a pilot experiment, we consistently
147 found weaker depletion phenotypes using an *nhr-23::GFP::AID*::3xFLAG* strain (Ragle
148 et al., 2020) compared to the *nhr-23::AID*::3xFLAG strain* (Zhang et al.,
149 2015)(unpublished data). We therefore transitioned to using the *nhr-23::AID*::3xFLAG*
150 strain for all experiments involving phenotypic analysis. We first tested NHR-
151 23::AID*::3xFLAG depletion kinetics and found near complete depletion within 15 minutes
152 after exposure to 4 mM auxin (Fig 2B).
153
154 We then performed timed depletion experiments in the L1 larval stage (Fig. 2A), similar
155 to those used to determine the role of NHR-23 in spermatogenesis (Ragle et al., 2020).
156 Experiments were conducted with an *eft-3p::TIR1::mRuby2* control strain (henceforth
157 referred to as *TIR1*) and a strain that permits somatic depletion of NHR-23 in the presence
158 of auxin, (*eft-3p::TIR1::mRuby2; nhr-23::AID*::3xFLAG;* henceforth referred to as *nhr-*
159 *23::AID*; *TIR1*). Synchronized L1s were shifted onto either 4 mM auxin or control plates
160 every two hours (Figure 2A). Animals were scored for molting defects at 20 hours post-
161 release. 100% of *TIR1* control animals shifted onto control or auxin plates successfully
162 molted and transitioned into the second larval stage. *nhr-23::AID*; *TIR1* animals shifted
163 onto control plates also reached the L2 stage, indicating that ethanol does not affect
164 developmental timing in this context. In contrast, *nhr-23::AID*; *TIR1* animals shifted onto
165 auxin displayed multiple phenotypes including larval arrest, molting defects, vacuoles,
166 developmental abnormalities such as disrupted tails and viable animals with a squashed
167 morphology ("splatter")(Fig. 2C). We then quantified the molting defects, scoring animals
168 unable to shed their cuticles, or with morphological abnormalities (Fig. 2D). Vacuoles
169 were observed in both the *TIR1* control and *nhr-23::AID; TIR1* strains. This could be a
170 result of exposure to auxin or possibly an effect of the imaging process. We did not pursue
171 the vacuole phenotype further. The percentage of *nhr-23::AID*; *TIR1* animals with molting
172 defects were low (0-5%) when animals were shifted to auxin between 2-4 hours post

173 release (Fig. 2D). However when *nhr-23::AID; TIR1* animals were shifted 6-12 hours post
174 release we observed a higher penetrance of molting defects (28-58%)(Fig. 2D). These

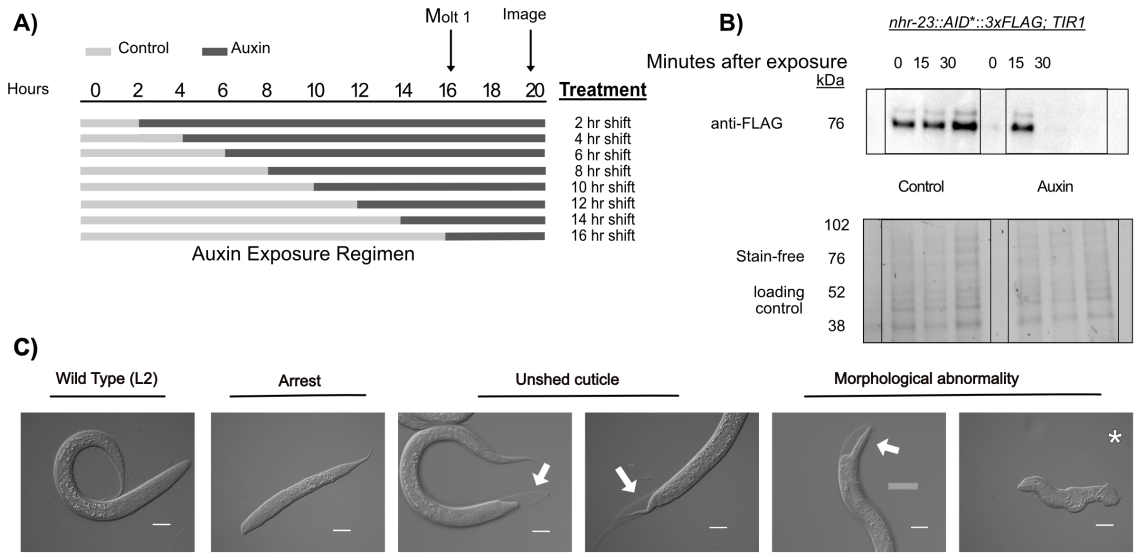

D) Phenotypic data for *nhr-23::AID; TIR1*

Shift Hour	(n)		% Unshed cuticle		% Morphological abnormality	
	nhr-23::AID; TIR1	*TIR1*	*nhr-23::AID; TIR1*	*TIR1*	*nhr-23::AID; TIR1*	*TIR1*
2	*40*	*40*	0	*0*	5	*0*
4	*40*	*40*	28	*0*	5	*0*
6	*40*	*31*	40	*0*	18	*0*
8	*40*	*35*	40	*0*	30	*0*
10	*31*	*37*	58	*0*	42	*0*
12	*40*	*20*	40	*0*	55	*0*
14	*39*	*32*	5	*0*	0	*0*
16	*40*	*36*	5	*0*	5	*0*

Figure 2: Distinct phenotypes are observed when NHR-23 is depleted early or late in L1 larvae. (A) Schematic of the experimental set-up. Synchronized L1 larvae were grown on control media (light grey bands) and transferred to 4mM auxin (dark grey bands) every 2 hours. Animals remained on auxin until they were imaged at 20 hours post-release. (B) Anti-FLAG immunoblot to monitor the speed of NHR-23 depletion. Synchronized *nhr-23::AID*::3xFLAG; TIR1* and *TIR1* animals were grown on MYOB plates for 12 hours, which corresponded to the peak in L1 expression from Figure 1C. Animals were then shifted onto control or auxin plates and lysates were collected at 15 and 30 minutes post-exposure. Marker size (in kDa) is provided. Stain-free analysis, which visualizes total protein on the membrane, is provided as a loading control. (C) Representative images of phenotypes observed when *nhr-23::AID*::3xFLAG; TIR1* animals were exposed to auxin in the first larval stage. (D) Percent of animals of the indicated genotypes with unshed cuticles and morphological abnormalities following exposure to auxin. The number of animals scored (n) is provided.

175 data could suggest that NHR-23 may not be necessary for the initiation of the molt but
176 required for completion of the molt. Additionally, the majority of *NHR-23::AID; TIR1*
177 animals shifted on to auxin at the 14 and 16 hour time points appeared wild type (Fig.
178 2D). *TIR1* and *nhr-23::AID; TIR1* animals grown on control plates developed normally
179 with no arrest or morphological defects (N=35 for each strain). We repeated the 16 hour
180 shift experiment and scored animals 48 hours later. Based on size, gonadal morphology,
181 and vulval morphology, animals arrested in L2 and L3 (Figure S3). Thus depletion of
182 NHR-23 during the final 2 hours of the L1 larval stage did not disrupt molting, suggesting
183 that NHR-23 is not necessary during this window to complete the molt to L2.
184
185 *Tissue-Specific NHR-23 depletion*
186 We next wanted to explore the observed molting phenotypes and further identify in which
187 tissues NHR-23 is necessary for completion of the molt. In addition to being expressed in
188 seam and hypodermal cells (Fig. S1), single-cell RNA-seq data indicates that *nhr-23* is
189 also expressed in rectal cells, vulval precursor cells, excretory cells (likely duct and pore
190 cells), and glial socket cells (Cao et al., 2017). We performed auxin depletion experiments
191 with a panel of recently described tissue-specific TIR1 transgenes developed for
192 hypodermal (*col-10p*), intestinal (*ges-1p*), neuronal (*rgef-1p*), seam cell (SCMmin
193 enhancer+*pes-10delta* minimal promoter) and multi-tissue depletion (*vha-8p:* seam cell,
194 hypodermis, gut, excretory cell, unidentified head cells)(Ashley et al., 2021). Surprisingly,
195 no phenotypes were observed when NHR-23 was depleted using hypodermal-, intestinal-
196 , neuronal- or seam cell-specific *TIR1* transgenes. Only depletion using the *vha-8*p*::TIR1*
197 transgene was able to phenocopy the pan-somatic *TIR1* allele (*eftp::TIR1*) (Table 1).
198 These data could reflect: i) incomplete depletion of NHR-23 in hypodermis, intestine,
199 neurons, or seam cells; ii) NHR-23 is not necessary in those cell types; iii) NHR-23 activity
200 is required in multiple tissues, with single-tissue depletion being insufficient to disrupt
201 molting.
202

Tissue specific depletion of NHR-23

TIR1 Promoter	Tissue	Larval Arrest	Molt Defects
col-10	*hypodermis*	no	no
rgef-1	*neurons*	no	no
vha-8	*neurons, gut, hypodermis*	yes	yes
SCMmin + pes-10	*seam cells*	no	no

Depletion of NHR-23 leads to a defective cuticle barrier

We next tested the function of the epidermal barrier using an *nlp-29p::GFP* reporter. *nlp-29* is an antimicrobial peptide expressed following wounding or exposure to particular pathogens (Pujol et al., 2008). Mutations or RNAi that alter the cuticle barrier also trigger *nlp-29* expression (Dodd et al., 2018; Melo and Ruvkun, 2012; Sandhu et al., 2021; Ward et al., 2014, 25). Given the mild morphological and molting defects observed following early NHR-23 depletion in L1 larvae, we reasoned that the cuticle barrier might be intact. The *TIR1* control only had weak *nlp-29p::GFP* expression which was not noticeably different between control and auxin treated animals (Fig. 3A,B). The *nhr-23::AID, TIR1* animals on control media had slightly elevated levels of *nlp-29p::GFP* on control media. In contrast, both early and late exposure of *nhr-23::AID, TIR1* animals to auxin caused the reporter to be overexpressed, suggesting hypodermal damage in both cases (Fig. 3A,B). We further tested the cuticle integrity in a hypo-osmotic shock assay in which animals with defective cuticle barriers rapidly die following exposure to water (Kage-Nakadai et al., 2010). As this assay typically scores L4s or adults, we grew animals to early L3 (25 hours post-release), shifted animals onto control or auxin plates, and tested sensitivity to hypo-osmotic stress. *TIR1* animals grown on control media or auxin were completely viable in water (Fig. 3C). *nhr-23::AID, TIR1* control animals had a weakly penetrant sensitivity to hypo-osmotic shock, while the same strain grown on auxin rapidly died following hypo-osmotic shock (Fig. 3C). Similarly, *nhr-23::AID, TIR1* control animals also had mildly elevated *nlp-29p::GFP* expression, which may suggest the strain is a

225 weak hypomorph. Together, the data suggest that NHR-23 is required for maintenance
226 of the cuticle barrier.

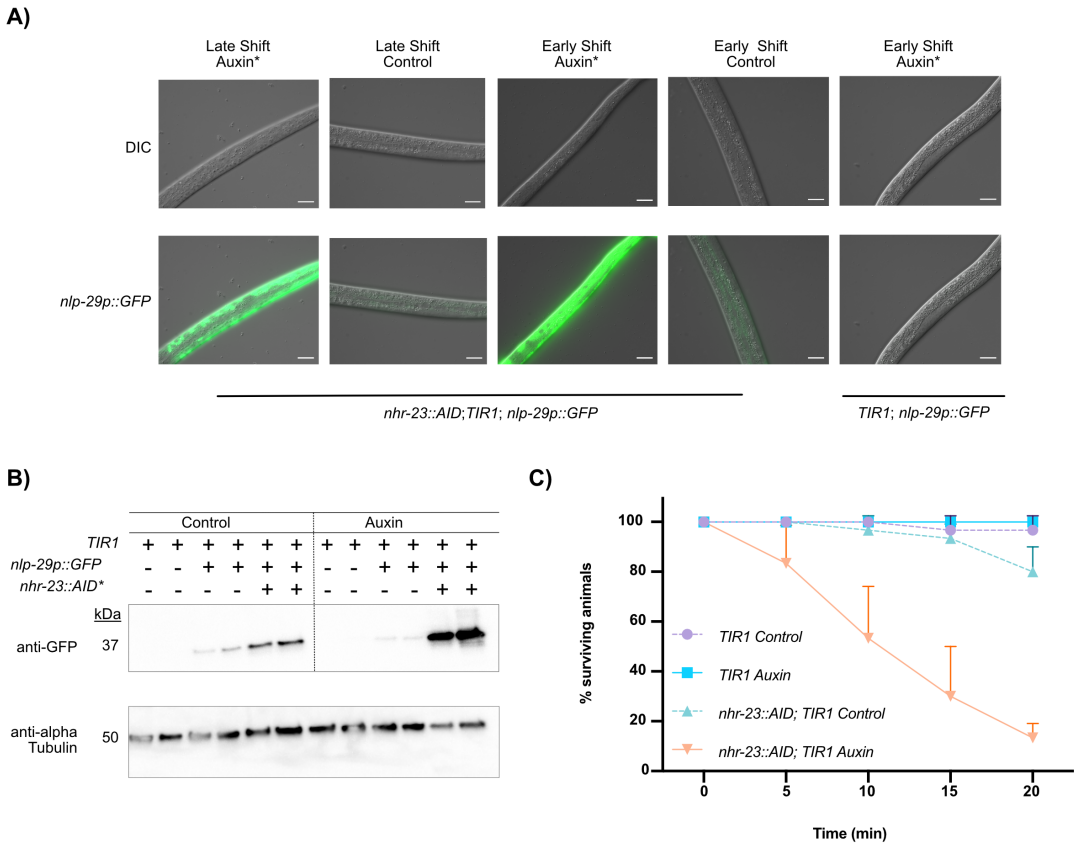

Figure 3: Depletion of NHR-23 leads to a defective cuticle barrier (A and B) Animals expressing *nlp-29::*GFP were crossed to *nhr-23::AID**::3xFLAG; TIR1 and TIR1 animals. (A) Representative images of GFP expression in animals of the indicated genotype following an early and late shift to control or auxin plates.(B) Anti-GFP immunoblot analysis of *nlp-29::*GFP expression. Marker size (in kDa) is provided. Stain-free analysis, which visualizes total protein on the membrane, is provided as a loading control. (C) *nhr-23::AID**::3xFLAG;TIR1 and TIR1 animals were added to 20µl of dH_20 and viability was assessed every five minutes. 10 animals were assayed for each genotype and condition with three biological replicates.

227

228 *NHR-23 depletion causes larval arrest*

229 *nhr-23::AID*; *TIR1* animals exposed to auxin at hours 2 and 4 appeared smaller than
230 control animals, suggesting a potential developmental arrest. This arrest was not
231 reversed by removing animals from auxin (unpublished data). Notably, *nhr-23(tm1323)*
232 null homozygotes are reported to arrest in L1 and L2, however the parameters used to

233 define these arrest points were not defined (Kouns et al., 2011). To test whether NHR-23
234 depletion triggers a developmental arrest, we used an *hlh-8p::GFP* promoter reporter to
235 monitor the M lineage (Harfe et al., 1998). Newly hatched L1 animals have one M cell
236 which undergoes a stereotypical series of divisions to produce 16 M lineage cells by the
237 L1 molt (Fig. 4A)(Sulston and Horvitz, 1977). To determine whether animals were
238 arresting in the L1 stage, we shifted synchronized *nhr-23::AID*; *TIR1* animals carrying an
239 *hlh-8p::GFP* reporter onto auxin plates at 3 hours and 9 hours post-release. We imaged
240 animals 24 hours post-release and M cell number was scored. *nhr-23::AID*; *TIR1* animals
241 exposed to auxin 3 hours post-release had an average count of 13.45 M cells (95%
242 confidence interval=0.6) while the late exposure resulted in an average of 15.55 M cells
243 (95% confidence interval=0.3)(Fig. 4B). As auxin concentrations of 1 mM and above can
244 slow *C. elegans* development (Zhang et al., 2015), we shifted *TIR1, hlh-8p::GFP* animals
245 onto auxin at 3 hours and confirmed that they had a similar number of M cells to animals
246 grown on control plates (Fig. 4B). This difference was statistically significant (two-tailed t-
247 test $p=8x10^{-8}$). The *nhr-23::AID*; *TIR1* animals exposed to auxin 9 hours post release did
248 not have significantly different M cell number than any of the controls ($p>0.3$)(Fig. 4B).
249 We also observed that the *nhr-23::AID*; *TIR1, hlh-8p::GFP* animals exposed to auxin at
250 three hours displayed more penetrant molting defects compared to the strain lacking the
251 *hlh-8p::GFP* reporter (unpublished data). This result could indicate that the *hlh-8p::GFP*
252 or the *dpy-20(+)* marker in the integrated transgene may be suppressing the larval arrest
253 phenotype caused by early depletion of NHR-23 in L1 larvae. Regardless, the M cell
254 reporter data indicates that depletion of NHR-23 3 hours post-release causes an L1
255 arrest.
256
257 To test whether this arrest due to early NHR-23 depletion was unique to the L1 stage, we
258 performed similar depletion experiments shifting early L3 animals onto auxin and
259 monitoring development by scoring vulva morphology 24 hours later (Mok et al., 2015).
260 While NHR-23 is expressed in vulval precursor cells, we never saw aberrations in vulval
261 morphology in *nhr-23::AID, TIR* animals grown on auxin.The majority of TIR1 animals
262 developed to late L4, with auxin causing a slight developmental delay evidenced by more
263 animals in mid-L4. *nhr-23::AID*; *TIR1* animals grown on control plates also reached late

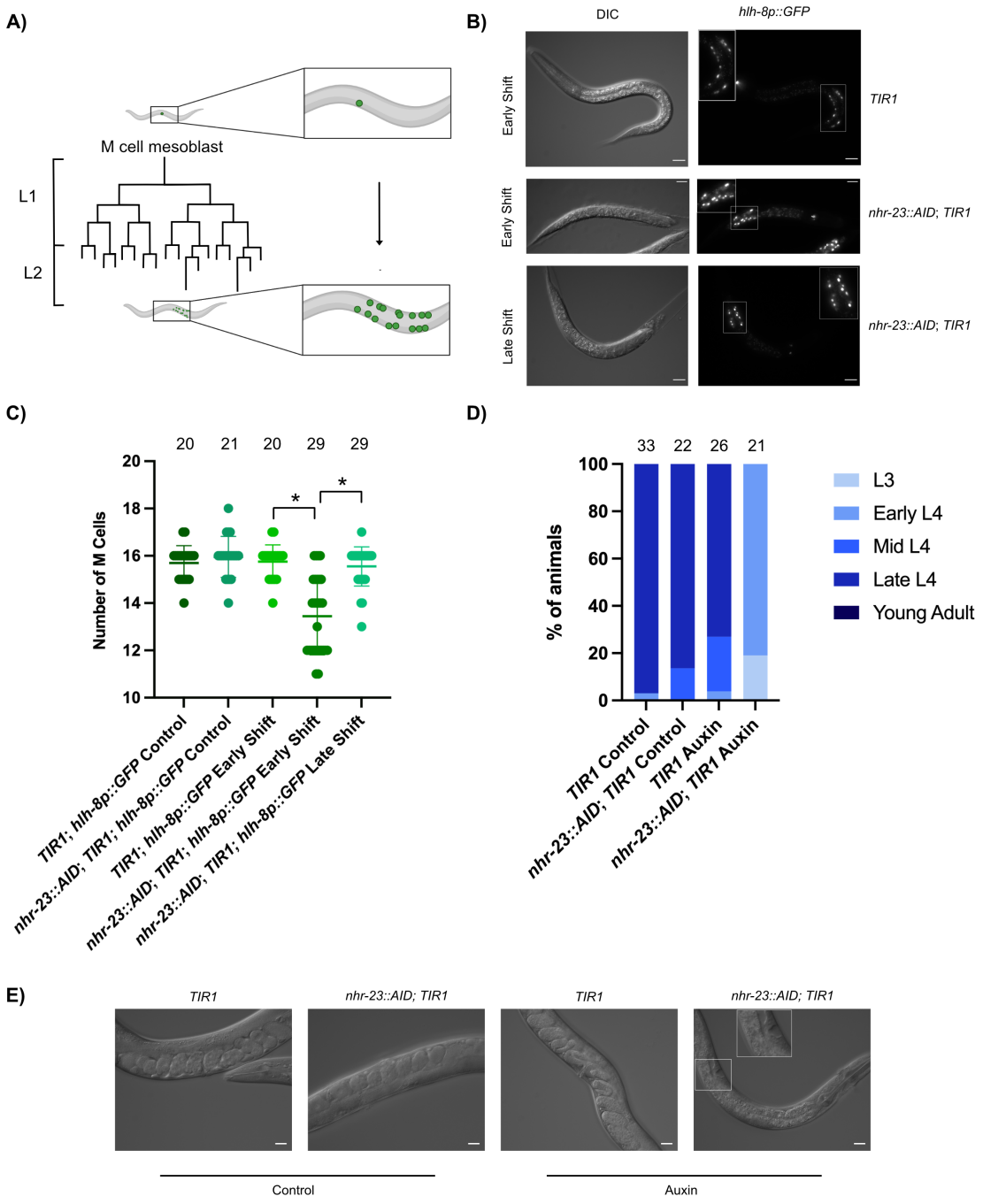

Figure 4: NHR-23 depletion causes larval arrest. (A) Depiction of the M cell mesoblast cell divisions in L1 larvae created with BioRender.com. Newly hatched animals are born with a single M cell, which undergoes the indicated set of divisions to produce 16 descendents at the L1/L2 molt. An *hlh-8p::GFP* reporter can be used to monitor M cell divisions in living animals. (B and C) Animals of the indicated genotype were synchronized and shifted to either auxin or control plates at either 3 (early shift) or 9 hours (late shift) post-release and imaged at 24 hours post-release. (B) Representative images of animals of the indicated genotypes on auxin plates. (C) M cell quantification for animals of the indicated genotype shifted to control or auxin plates. Mean and standard deviation are labeled. The number of animals assayed for each genotype and condition is indicated at the top of the graph.

Fig 4 legend, continued

(D) Animals of the indicated genotype were synchronized and shifted onto auxin at 25 hours post-release and imaged 23 hours later (48 hours post-release). Animals were staged based on vulval morphology (Mok et al., 2015). L4 larval stages were grouped as Early L4 (4.0-4.2), Mid L4 (4.3-4.5), and Late L4 (4.6-4.9). The number of animals assayed for each genotype and condition is indicated at the top of the graph. (E) In a repeated experiment animals were synchronized and shifted onto auxin at 25 hours post-release and imaged 48 hours post shift. Representative images of vulva stages observed in animals for each indicated genotype and condition.

265 mid-L4. In contrast, when *nhr-23::AID*; *TIR1* animals were shifted to auxin, the vast
266 majority of animals were arrested in early L4 with a fraction of the population remaining
267 in L3. Repeating the experiment and scoring developmental progression 48 hours post
268 shift to control or auxin plates confirmed that *nhr-23::AID*; *TIR1* animals grown on auxin
269 were arrested predominantly in L4 (representative image in Fig 4E). *TIR1* animals on
270 either control or auxin plates and *nhr-23::AID*; *TIR1* animals on control plates all reached
271 adulthood (unpublished data. These data indicate that NHR-23 activity is required in
272 multiple larval stages for developmental progression.
273
274 *Larval arrest following NHR-23 depletion is independent of the insulin signaling pathway*
275 There are well-characterized developmental checkpoints that promote larval arrest in the
276 absence of food (Fielenbach and Antebi, 2008; Kaplan and Baugh, 2016). *daf-16* is a
277 transcription factor which is part of the insulin signaling pathway and is necessary for
278 starvation-induced L1, L3, and L4 arrest (Baugh and Sternberg, 2006; Schindler et al.,
279 2014). Starved *daf-16* mutants fail to arrest at these checkpoints and continue
280 development (Baugh and Sternberg, 2006; Schindler et al., 2014). We crossed a *daf-*
281 *16(mu86)* null allele into our *TIR-1; hlh-8p::GFP* and *nhr-23::AID; TIR1; hlh-8p::GFP*
282 strains and grew synchronized L1 larvae on control or auxin plates. *daf-16(mu86), TIR1*
283 animals were able to reach adulthood on both control and auxin plates. *nhr-23::AID, TIR1,*
284 *daf-16(mu86)* animals reached adulthood on control plates, but were arrested as larvae
285 when grown on auxin. To determine whether this arrest was in L1, we repeated this
286 experiment and monitored the myoblast lineage. *nhr-23::AID, TIR1, daf-16(mu86)*
287 animals shifted onto control plates had similar M cell counts to *TIR1, daf-16(mu86)*
288 animals grown on either control or auxin plates (Fig. 5A). These M cell counts were
289 consistent with animals having made it to the L1 molt. In contrast, *nhr-23::AID, TIR1, daf-*

290 *16(mu86)* animals shifted onto auxin averaged 12.85 M cells (95% confidence
291 interval=2), which was significantly different from the controls (two-tailed t-test $p=4x10^{-7}$)
292 and indicative of a larval arrest (Fig. 5A).
293
294

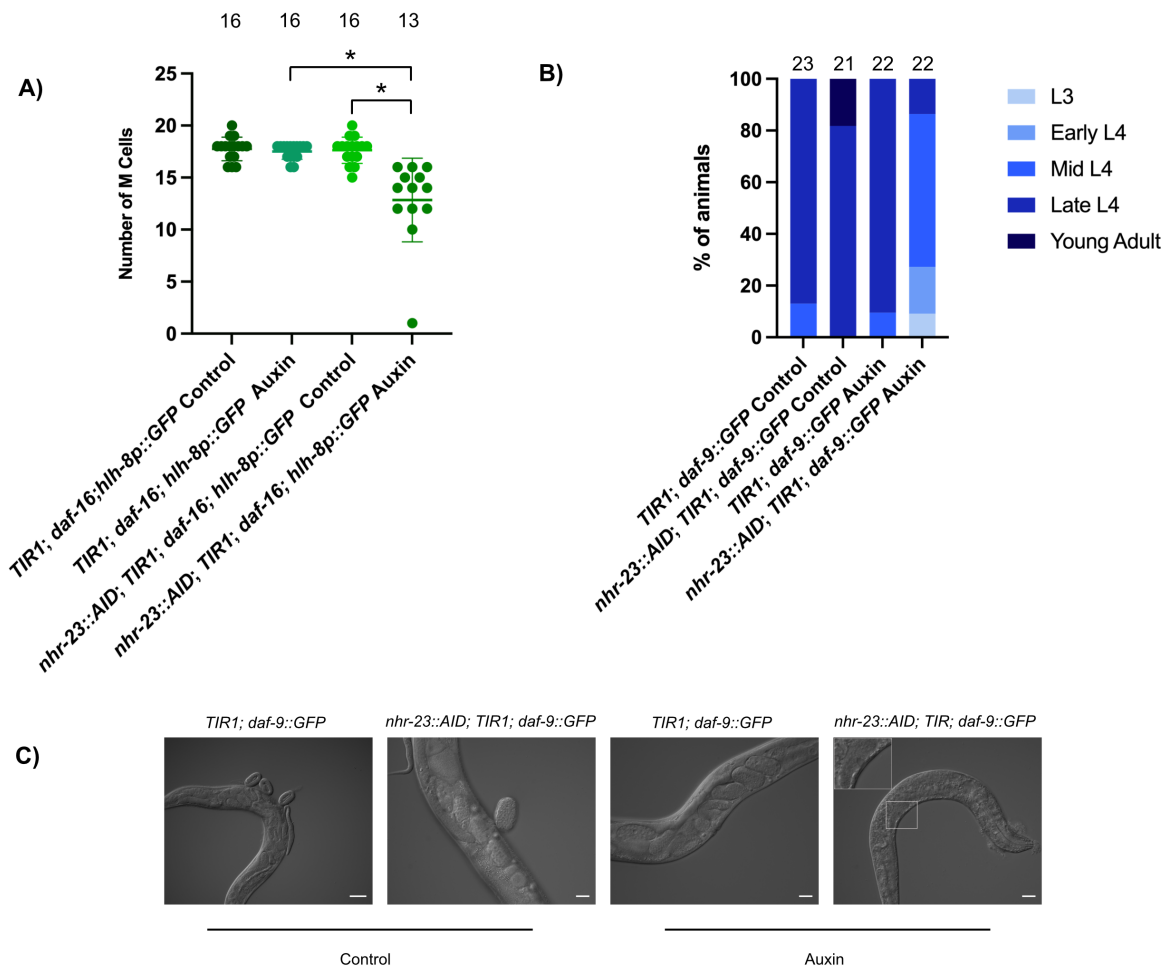

Figure 5: Larval arrest following NHR-23 depletion is *daf-16*-independent, but partially suppressed by *daf-9* overexpression. (A) M cell quantitation for synchronized animals of the indicated genotype shifted to auxin plates at 3 hours post-release and imaged 21 hours later (24 hours post-release). Mean and standard deviation labeled. The number of animals assayed for each genotype and condition is indicated at the top of the graph.(B and C) Animals of the indicated genotype were synchronized and shifted onto auxin at 25 hours post-release and imaged 23 hours later (48 hours post-release). Animals were staged based on vulval morphology (Mok et al., 2015). L4 larval stages were grouped as Early L4 (4.0-4.2), Mid L4 (4.3-4.5), and Late L4 (4.6-4.9). The number of animals assayed for each genotype and condition is indicated at the top of the graph. (C) Representative images of vulva stages 73 hours post release.

295 Overexpression of the cytochrome P450 gene *daf-9* (*daf-9::GFP*) was shown to act in the
296 *daf-16* pathway and produce an even more robust bypass of the L3 and L4 nutritional
297 checkpoint (Schindler et al., 2014). This strain overexpresses *daf-9::GFP* in the two
298 endocrine XXX cells, though under starvation conditions *daf-9::GFP* will be
299 overexpressed in the hypodermis (Gerisch et al., 2001). NHR-23 depletion did not trigger
300 *daf-9::GFP* hypodermal expression, suggesting that animals were not starving (Fig. S4).
301 The majority of *TIR1; daf-9::GFP* animals shifted to control or auxin plates in early L3
302 reached the late L4 stage (Fig. 5C). Similarly, *nhr-23::AID, TIR; daf-9::GFP* animals
303 shifted onto control plates reached the late L4 stage (Fig. 5C). When *nhr-23::AID, TIR;*
304 *daf-9::GFP* animals were shifted onto auxin the majority of animals were in mid-L4, with
305 a smaller fraction of the population in L3, early L4, or late L4 (Fig. 5C). When we repeated
306 the experiment and scored animals 48 hours after the auxin shift, *nhr-23::AID, TIR; daf-*
307 *9::GFP* animals were still in early to mid L4 suggesting that we were observing an arrest
308 rather than developmental delay (representative image in Fig. 5C). Repeating the
309 experiment and scoring animals 48 hours post-shift onto control or auxin plates confirmed
310 that *nhr-23::AID, TIR; daf-9::GFP* animals were arresting in L4 on auxin plates. While
311 *daf-9::GFP* overexpression allowed animals to progress later in L4 compared to NHR-23
312 depletion alone, these animals never molted into young adults and we classified this
313 phenotype as an L4 arrest. These results suggest that the larval arrest caused by NHR-
314 23 depletion is independent of the insulin signaling pathway.
315
316 *NHR-23 regulates oscillating genes involved in aECM biogenesis, lipid transport, and*
317 *signal transduction*
318 To gain insight into how depletion of NHR-23 at different points in larval development
319 affects molting, we analyzed the expression of NHR-23-regulated genes by mining
320 existing microarray (Kouns et al., 2011) and oscillatory gene expression data (Hendriks
321 et al., 2014)(Table S1). Of the 265 NHR-23 regulated genes, 236 (89%) were oscillatory
322 (Table S1); a similar trend was observed in a recent analysis of these datasets (Tsiairis
323 and Großhans, 2021). In contrast, 10-20% of *C. elegans* genes oscillate in expression
324 (Hendriks et al., 2014; Kim et al., 2013; Meeuse et al., 2020)(Two-tailed Chi-squared test
325 $p<0.0001$). To test whether these *nhr-23*-regulated oscillating genes were enriched for

326 particular biological functions, we performed gene ontology analysis which indicated an
327 enrichment in genes implicated in: i) molting and/or cuticle structure; ii) lipid metabolism
328 and transport; iii) protease inhibition; iv) cell adhesion; and v) protein autoprocessing
329 (genes related to hedgehog signaling)(Fig. S5). Interestingly, while the *C. elegans*
330 genome encodes 181 collagen genes (Teuscher et al., 2019), *nhr-23* only regulated 13
331 collagens but these include all of the furrow collagens implicated in epidermal damage
332 sensing (Table S1; *dpy-2, dpy-3, dpy-7, dpy-10*)(Dodd et al., 2018). Other regulated
333 collagens have well-described roles in body morphology (*sqt-1, sqt-2, rol-6*)(Kramer and
334 Johnson, 1993). There are also several sets of genes involved in apical extracellular
335 matrix biogenesis and remodeling, such as lipocalins, proteases, protease inhibitors,
336 fibrillin, PAN and ZP domain-containing proteins, and leucine-rich repeat proteins.
337 Although not enriched as a gene ontology class, NHR-23 also regulates several
338 transcription factors implicated in molting or energy metabolism (*peb-1, nhr-91, dpy-*
339 *20*)(Clark et al., 1995, 20; Fernandez et al., 2004; Kasuga et al., 2013). Most of the genes
340 in these ontology classes have a peak phase following that of *nhr-23* (Fig. 6C).
341 (modENCODE Consortium et al., 2010). As expected, NHR-23 was enriched in the
342 promoter region of genes (Fig. S6). There was also notable enrichment downstream of
343 the transcriptional end site (Fig. S6). We then examined whether NHR-23 was enriched
344 near *nhr-23*-regulated oscillating genes. We converted the period to developmental time
345 assuming a 9 hour larval stage which makes each hour equivalent to 40º. We separated
346 the genes into three groups based on their peak phase. There were low levels of NHR-
347 23 binding in genes that peaked in expression between 0 and 3 hours (Fig. 6B). For
348 reference, *nhr-23* peaks at 178.11º/4.45 hours (Meeuse et al., 2020). In contrast, the
349 genes that peaked in expression between 3 and 6 hours had much higher NHR-23 binding
350 (Fig. 6B). The genes peaking in expression later (6-9 hours) had reduced NHR-23
351 binding, but still higher levels than the genes peaking between 0 and 3 hours (Fig. 6B).
352 Thus genes which peak in expression close to when *nhr-23* mRNA levels peak tend to
353 have higher NHR-23 levels upstream, downstream, and within their gene bodies (Fig.
354 6B).
355

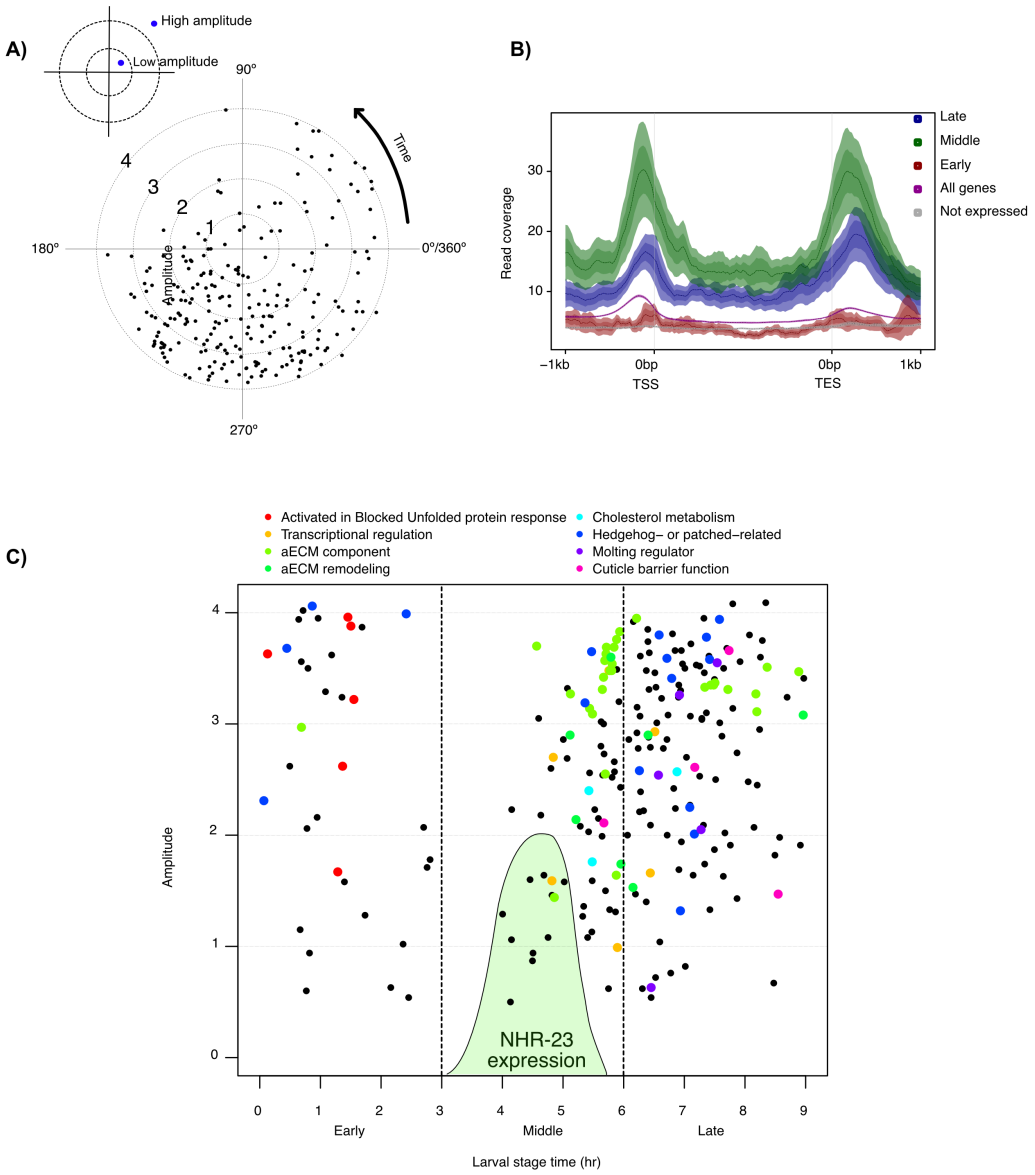

Figure 6: NHR-23 regulates oscillating genes involved in aECM biogenesis, lipid transport, and signal transduction. (A) A radar chart plotting amplitude over the phase of peak expression of *nhr-23*-regulated genes from Kouns *et al.* (2011). The dotted circles indicated amplitude, with the innermost circle representing an amplitude of 1 and the outermost circle representing an amplitude of 4. (B) Average signal from NHR-23 ChIP-seq data for *nhr-23*-regulated oscillating genes which peak phases between 0º-120º (Early), 120-240º (Middle), and 240º-360º. For reference, *nhr-23* mRNA peaks at 178.11º. The average NHR-23 signal for all 21,600 *C. elegans* genes (All genes) and the 20% of genes with the lowest expression (No expression) are shown for reference. The mean signal is plotted with a line and the mean's 95% confidence interval is indicated by the shaded area. (C) The data from (A) was plotted as a scatter plot and functionally annotated (see Table S1). To provide developmental context, we converted the 360º oscillation to developmental timing over a 9 hour larval stage, such as the L3 or L4 stage at 20ºC. In this context, 1 hour=40º and this converted developmental time is used in B and C. *nhr-23* mRNA has a peak phase of 178.11º (4.45 hours) with an amplitude of 2.11 (Meeuse et al., 2020).The green shaded area represents NHR-23 expression based on RNA-seq (Meeuse et al., 2020), imaging (Figure 1B), and western blotting data (Figure 1C). Dotted lines indicate boundaries between the early, middle, and late *nhr-23*-regulated oscillating genes from B.

357 **Discussion**

358 *C. elegans* molting is a powerful model to understand how a large-scale gene oscillator
359 is integrated into rhythmic epidermal regeneration. In this study, we identify distinct
360 windows of NHR-23 activity required for initiation and execution of the molt program and
361 formation of the epithelial barrier.

362

363 *A model for the role of NHR-23 in molting*

364 Depletion of NHR-23 early in a larval stage before NHR-23 levels start rising produces a
365 larval arrest with only weakly penetrant molting defects (Fig 2). In contrast, depletion after
366 NHR-23 levels have risen produces molting and developmental defects (Fig. 2). The first
367 larval stage appeared to be most sensitive to NHR-23 depletion, as all animals appeared
368 to arrest in the L1 stage. In contrast, depletion at the start of L2 produced arrests in both
369 L2 and L3 larvae, and depletion at the start of L3 produced arrests in L3 and L4 larvae. It
370 is unclear whether these differences are technical, such as NHR-23 depletion is more
371 effective in L1 because of smaller animal volume or the longer duration of the L1 stage
372 affords more time to deplete NHR-23 below a critical threshold. Alternatively, NHR-23
373 might play a more prominent role in L1 vs other larval stages.

374

375 Larval arrest following NHR-23 depletion was not suppressed by *daf-16* inactivation, so
376 is not an insulin/IGF-regulated development checkpoint. There were no molting defects
377 nor arrests observed when animals were exposed to auxin following the NHR-23 peak in
378 expression, suggesting that these animals were able to molt and arrest in the next larval
379 stage. NHR-23 depletion phenotypes might represent defects in molting initiation (early
380 depletion) or molting execution (late depletion). The arrest caused by early NHR-23
381 depletion might reflect failure to activate the next tier of a gene regulatory program. This
382 model would be consistent with insect molting, in which the hormone ecdysone triggers
383 a regulatory cascade driven by nuclear hormone receptors, including the NHR-23
384 ortholog DHR3 (King-Jones and Thummel, 2005; Lam et al., 1997; Ruaud et al., 2010;
385 Thummel, 1990). Consistent with this model, *nhr-23* regulates *peb-1* and *dpy-20*,
386 transcription factors with known roles in molting (Clark et al., 1995, 20; Fernandez et al.,
387 2004, 1). *nhr-23* also regulates *nhr-91* (Kouns et al., 2011)(Table S1), a nuclear hormone

388 receptor involved in blast cell progression in response to nutrients (Kasuga et al., 2013).
389 An alternate, non-exclusive model is that physiological defects trigger an arrest. Early
390 *nhr-23*-regulated genes include a set of apical ECM components required to preserve
391 epithelial integrity during morphogenesis (*fbn-1, sym-1, let-4, noah-1, noah-2*)(Kelley et
392 al., 2015, 1; Vuong-Brender et al., 2017). An equivalent structure may be required in
393 larvae prior to apical ECM remodeling to ensure that the internal turgor pressure does not
394 cause epithelial rupture. One intriguing possibility is that the earlier NHR-23-regulated
395 genes may be more sensitive to NHR-23 levels. This model would align with *E. coli* amino
396 acid biosynthesis gene regulation where enzymes earlier in the pathway have more
397 responsive promoters with higher activity (Zaslaver et al., 2004). Accordingly, there is an
398 enrichment for NHR-23 binding flanking and within oscillating genes that peak in
399 expression close to the NHR-23 peak in expression (Fig. 6B). However, formal testing of
400 this model would require an intensive study involving biochemical assessment of NHR-
401 23 affinity for candidate binding sites and experimental manipulation *in vivo* of the
402 candidate binding sites.
403
404 Later depletion of NHR-23 might allow the molt to initiate, but the loss or reduction of
405 critical aECM components and remodeling factors, signaling proteins, and metabolic
406 enzymes could cause the molt to fail resulting in the observed developmental and ecdysis
407 defects (Fig. 6C). *nhr-23* regulates the expression of five lipocalin genes all peaking within
408 a 15º period (equivalent to 15 minutes in a 9 hour larval stage)(Table S1). Two of these
409 lipocalins (LPR-1 and LPR-3) are required for aECM organization, with LPR-3 playing an
410 additional role in ecdysis (Forman-Rubinsky et al., 2017). Some lipocalins can bind matrix
411 metalloproteases (Leng et al., 2009; Yan et al., 2001). Notably, *nhr-23* also regulates *nas-*
412 *37*, a conserved matrix metalloprotease with roles in ecdysis (Davis et al., 2004) as well
413 as two uncharacterized predicted proteases (*nas-4, spg-7*). Metalloprotease activity must
414 presumably be tightly regulated to prevent premature ecdysis. *mlt-11* is a poorly
415 characterized protease inhibitor with nine Kunitz protease inhibitor domains, and peaks
416 in expression prior to these proteases so might function to regulate the timing of ecdysis.
417 *nhr-23*-regulated genes predicted to function in lipid metabolism or transport could also
418 contribute to the late NHR-23 depletion phenotype. There are a number of hedgehog-

419 related (*qua-1, wrt-1, wrt-4*) and Patched or Patched-related genes (*ptc-3, ptr-4, ptr-10,*
420 *ptr-11, ptr-18*), a subset of which are implicated in molting or lipid transport (Chiyoda et
421 al., 2021, 4; Cohen et al., 2021, 4; Hao et al., 2006; Zugasti et al., 2005). It has been
422 hypothesized that a sterol ligand regulates nematode molting as cholesterol depletion in
423 *C. elegans* phenocopies *nhr-23* inactivation and insect molting is initiated by a pulse of
424 the steroid hormone ecdysone(Lažetić and Fay, 2017; Thummel, 1990); *nhr-23* regulates
425 two genes predicted to be involved in steroid metabolism (*dhs-16, mboa-1)*(Kouns et al.,
426 2011)(Table S1). Future analysis of these candidate *nhr-23* targets will illuminate how
427 collagen secretion, apical ECM remodeling, apolysis, and ecdysis are coordinated with
428 developmental progression.
429
430 *NHR-23 is necessary for epithelial barrier establishment and/or maintenance*
431 Early NHR-23 depletion caused sensitivity to hypo-osmotic stress and activation of an
432 *nlp-29p::GFP* reporter (Fig 3). These data suggest that despite looking superficially wild-
433 type that there are cuticular abnormalities. There are numerous *nhr-23*-regulated genes
434 which are implicated in the epithelial barrier. The cuticle furrow formed by six *nhr-23*-
435 regulated collagens (*dpy-2, dpy-3, dpy-7, dpy-8, dpy-9, dpy-10*) is thought to be monitored
436 by a sensor which coordinates a number of stress responses following detection (Dodd
437 et al., 2018). An RNAi screen of 91 collagens found that inactivation of only these six
438 collagens caused a barrier defect (Sandhu et al., 2021). Inactivation of a subset of the
439 furrow collagens also causes elevated *nlp-29p::GFP* reporter activity (Dodd et al., 2018),
440 consistent with our NHR-23-depletion data (Fig. 3). *bus-8* is a predicted
441 glycosyltransferase that plays a role in the epithelial barrier and is also *nhr-23*-regulated
442 and its peak expression follows that of the furrow collagens (Table S1). Screening *nhr-23*
443 regulated genes may find other genes implicated in the epithelial barrier and the peak
444 phase could provide insight into how this barrier is constructed.
445
446 *NHR-23 isoforms*
447 We detected three bands on our western blots, the size of which are consistent with
448 isoforms confirmed by Nanopore direct mRNA sequencing (NHR-23b/f, NHR-23c, NHR-
449 23e)(Roach et al., 2020). NHR-23b/f is predicted to contain an N-terminal extension with

450 an alpha helix and an unstructured domain not found in NHR-23c (Fig. S7,S8). In many
451 NHRs, unstructured regions in the N-termini, C-termini, or flexible region between the
452 DBD and LBD (hinge region) contain co-regulator docking sites (Krasowski et al., 2008).
453 It's possible that these isoforms form different transcriptional regulatory complexes.
454 Alternatively, the sequences flanking the DBD can impact binding site preference of
455 NHRs (Li et al., 2017; Simmons et al., 2008), meaning that these isoforms could regulate
456 different subsets of genes.
457
458 The most robustly expressed isoform is consistent with the size of NHR-23e, which peaks
459 prior to an abrupt decrease in all NHR-23 isoforms levels prior to the molt. NHR-23e lacks
460 all critical residues required for forming a functional DNA-binding domain, but contains
461 the hinge region and LBD (Fig. S7). A subset of *C. elegans* NHRs (36/278; Tables S2,3)
462 also have isoforms that lack DNA binding domains. This group includes 10 of the 34
463 functionally characterized NHRs, with several involved in nutrient sensing, dietary
464 restriction-mediated longevity, metabolism, and energy homeostasis (DAF-12, NHR-23,
465 NHR-25, NHR-49, NHR-62, NHR-68, NHR-91, NHR-114)(Antebi, 2015; Gerisch and
466 Antebi, 2004, 12; Gracida and Eckmann, 2013; Kasuga et al., 2013; Macneil et al., 2013;
467 Mullaney et al., 2010; Van Gilst et al., 2005a; Van Gilst et al., 2005b). While the function
468 of these DBDless isoforms in *C. elegans* has not been determined, they may function as
469 dominant-negative repressors. A well-characterized transcriptional regulatory mechanism
470 involves transcription factor dimerization where one of the monomers lacking a DBD can
471 still heterodimerize but serves as a "poison" subunit (Amoutzias et al., 2008).
472
473 *Is NHR-23 a cog in a gene expression oscillator?*
474 Recent work has revealed that ~10-20% of the *C. elegans* transcriptome undergoes
475 rhythmic oscillations, peaking each larval stage and likely controlling molting (Hendriks et
476 al., 2014; Kim et al., 2013; Meeuse et al., 2020). This process of rhythmic skin
477 regeneration has interesting parallels to postnatal mammalian hair follicle regeneration
478 as both involve non-circadian oscillations and are regulated by BLMP-1/BLMP1 (Hauser
479 et al., 2021; Paus and Foitzik, 2004; Stec et al., 2021). How the *C. elegans* gene
480 expression oscillator functions is only starting to be determined. The conserved

481 transcription factor BLMP-1/BLIMP1 shapes oscillatory gene expression (Hauser et al.,
482 2021) and acts as a pioneer factor to decompact chromatin (Stec et al., 2021). NHR-23
483 is a strong candidate to regulate a subset of molting genes in this oscillator. ChIP-seq
484 data indicates that BLMP-1 binds upstream of the NHR-23 transcription start site
485 (modENCODE Consortium et al., 2010). RNA-seq time courses indicate that *nhr-23* is
486 one of the earliest expressed transcription factors implicated in molting (Hendriks et al.,
487 2014; Meeuse et al., 2020). *nhr-23*-regulated genes are enriched for molting factors (Fig
488 6, Table S1)(Kouns et al., 2011), and 236 of the 265 NHR-23-regulated genes oscillate
489 (89%). The mammalian homolog of NHR-23 (RORalpha) regulates circadian rhythms,
490 and both NHR-23 and RORalpha proteins oscillate (Akashi and Takumi, 2005)(Figure 1).
491
492 Analysis of the *C. elegans* oscillator indicates that it operates on a Saddle Node on
493 Invariant Cycle (SNIC) bifurcation (Meeuse et al., 2020). An important characteristic of a
494 SNIC oscillator is arrest at specific phases, and the *C. elegans* oscillator can be arrested
495 at points corresponding with developmental checkpoints in each larval stage. Notably,
496 NHR-23 levels are at their lowest during these arrest points. Meeuse et al. hypothesized
497 that signals linked to metabolism or the nutrition state of the animal control the oscillator
498 at these checkpoints. Consistent with NHR-23 playing a role in the oscillator, it controls
499 developmental rate in response to diet likely through modulation of NHR-23 activity, not
500 levels (Macneil et al., 2013). Consistent with this model, the mammalian orthologs of
501 NHR-23 bind various sterol ligands (Kallen et al., 2002; Kallen et al., 2004; Soroosh et
502 al., 2014) and a ligand has been suggested to drive molting (Lažetić and Fay, 2017). A
503 SNIC oscillator is also characterized by interlinked positive and negative feedback loops.
504 In addition to the DBD-less isoform, which could function as a dominant negative
505 regulator, *nhr-23* is negatively regulated by the *let-7* microRNA and also positively
506 regulates this microRNA (Patel and Frand, 2018). This feedback loop represents a point
507 where the heterochronic pathway controlling developmental timing intersects with the
508 molting program. NHR-23 levels drop during the molt and NHR-23-depleted animals
509 shifted off auxin do not resume development, suggesting that NHR-23 is not likely
510 responsible for restarting the oscillation during a checkpoint but rather promoting

511 epidermal remodeling. Going forward, determining the factors that promote *nhr-23*
512 expression will be critical for defining how the oscillator functions.
513
514 **Future perspectives**
515 This work highlights the power of timed protein depletion for dissecting the role of
516 oscillating developmental regulators in development. We have found distinct phenotypes
517 depending on when we deplete NHR-23 in a given larval stage. Going forward it will be
518 important to determine whether NHR-23 acts cell-autonomously or non-autonomously,
519 and identify the critical tissues in which NHR-23 activity is necessary. As transcription
520 factors coordinate the expression of batteries of genes in a given biological process,
521 future work will reveal how NHR-23 coordinates apical ECM remodeling, apolysis, and
522 ecdysis. NHR-23 oscillates in the soma yet is constitutively expressed in the germline
523 (Ragle et al., 2020). Exploring the differences between oscillatory and constitutive NHR-
524 23 expression could shed light on mammalian gene regulation, as several circadian
525 rhythm regulators oscillate in the soma but are constitutively expressed in the testes
526 (Alvarez et al., 2008; Kang et al., 2010; Kennaway et al., 2012; Morse et al., 2003)
527
528 **References**
529
530 **Agbulut, O., Coirault, C., Niederländer, N., Huet, A., Vicart, P., Hagège, A., Puceat,**
531 **M. and Menasché, P.** (2006). GFP expression in muscle cells impairs actin-
532 myosin interactions: implications for cell therapy. *Nat. Methods* **3**, 331–331.
533 **Akashi, M. and Takumi, T.** (2005). The orphan nuclear receptor RORalpha regulates
534 circadian transcription of the mammalian core-clock Bmal1. *Nat. Struct. Mol. Biol.*
535 **12**, 441–448.
536 **Alvarez, J. D., Hansen, A., Ord, T., Bebas, P., Chappell, P. E., Giebultowicz, J. M.,**
537 **Williams, C., Moss, S. and Sehgal, A.** (2008). The circadian clock protein
538 BMAL1 is necessary for fertility and proper testosterone production in mice. *J.*
539 *Biol. Rhythms* **23**, 26–36.
540 **Amoutzias, G. D., Robertson, D. L., Van de Peer, Y. and Oliver, S. G.** (2008).
541 Choose your partners: dimerization in eukaryotic transcription factors. *Trends*

542 *Biochem. Sci.* **33**, 220–229.
543 **Antebi, A.** (2015). Nuclear receptor signal transduction in C. elegans. *WormBook* 1–49.
544 **Ashley, G. E., Duong, T., Levenson, M. T., Martinez, M. A. Q., Johnson, L. C.,**
545 **Hibshman, J. D., Saeger, H. N., Palmisano, N. J., Doonan, R., Martinez-**
546 **Mendez, R., et al.** (2021). An expanded auxin-inducible degron toolkit for
547 *Caenorhabditis elegans*. *Genetics* **217**, iyab006.
548 **Baens, M., Noels, H., Broeckx, V., Hagens, S., Fevery, S., Billiau, A. D.,**
549 **Vankelecom, H. and Marynen, P.** (2006). The Dark Side of EGFP: Defective
550 Polyubiquitination. *PLOS ONE* **1**, e54.
551 **Baugh, L. R. and Sternberg, P. W.** (2006). DAF-16/FOXO regulates transcription of
552 *cki-1*/Cip/Kip and repression of *lin-4* during *C. elegans* L1 arrest. *Curr. Biol.* **16**,
553 780–785.
554 **Blaxter, M. L.** (1993). Cuticle surface proteins of wild type and mutant *Caenorhabditis*
555 *elegans*. *J. Biol. Chem.* **268**, 6600–6609.
556 **Blaxter, M. L., Page, A. P., Rudin, W. and Maizels, R. M.** (1992). Nematode surface
557 coats: actively evading immunity. *Parasitol. Today Pers. Ed* **8**, 243–247.
558 **Brenner, S.** (1974). The genetics of *Caenorhabditis elegans*. *Genetics* **77**, 71–94.
559 **Bridgham, J. T., Eick, G. N., Larroux, C., Deshpande, K., Harms, M. J., Gauthier, M.**
560 **E. A., Ortlund, E. A., Degnan, B. M. and Thornton, J. W.** (2010). Protein
561 Evolution by Molecular Tinkering: Diversification of the Nuclear Receptor
562 Superfamily from a Ligand-Dependent Ancestor. *PLoS Biol.* **8**, e1000497.
563 **Campbell, L. A., Faivre, E. J., Show, M. D., Ingraham, J. G., Flinders, J., Gross, J.**
564 **D. and Ingraham, H. A.** (2008). Decreased Recognition of SUMO-Sensitive
565 Target Genes following Modification of SF-1 (NR5A1). *Mol. Cell. Biol.* **28**, 7476–
566 7486.
567 **Cao, J., Packer, J. S., Ramani, V., Cusanovich, D. A., Huynh, C., Daza, R., Qiu, X.,**
568 **Lee, C., Furlan, S. N., Steemers, F. J., et al.** (2017). Comprehensive single-cell
569 transcriptional profiling of a multicellular organism. *Science* **357**, 661–667.
570 **Chiyoda, H., Kume, M., Castillo, C. C. del, Kontani, K., Spang, A., Katada, T. and**
571 **Fukuyama, M.** (2021). *Caenorhabditis elegans* PTR/PTCHD PTR-18 promotes
572 the clearance of extracellular hedgehog-related protein via endocytosis. *PLOS*

573 *Genet.* **17**, e1009457.
574 **Church, D. L., Guan, K. L. and Lambie, E. J.** (1995). Three genes of the MAP kinase
575 cascade, *mek-2*, *mpk-1/sur-1* and *let-60 ras*, are required for meiotic cell cycle
576 progression in *Caenorhabditis elegans*. *Development* **121**, 2525–2535.
577 **Clark, D. V., Suleman, D. S., Beckenbach, K. A., Gilchrist, E. J. and Baillie, D. L.**
578 (1995). Molecular cloning and characterization of the *dpy-20* gene of
579 *Caenorhabditis elegans*. *Mol. Gen. Genet. MGG* **247**, 367–378.
580 **Cohen, J. D., Cadena del Castillo, C. E., Serra, N. D., Kaech, A., Spang, A. and**
581 **Sundaram, M. V.** (2021). The *Caenorhabditis elegans* Patched domain protein
582 PTR-4 is required for proper organization of the precuticular apical extracellular
583 matrix. *Genetics* iyab132
584 **Davis, M. W., Birnie, A. J., Chan, A. C., Page, A. P. and Jorgensen, E. M.** (2004). A
585 conserved metalloprotease mediates ecdysis in *Caenorhabditis elegans*.
586 *Development* **131**, 6001–6008.
587 **de Sousa Abreu, R., Penalva, L. O., Marcotte, E. M. and Vogel, C.** (2009). Global
588 signatures of protein and mRNA expression levels. *Mol. Biosyst.* **5**, 1512–1526.
589 **Dodd, W., Tang, L., Lone, J.-C., Wimberly, K., Wu, C.-W., Consalvo, C., Wright, J.**
590 **E., Pujol, N. and Choe, K. P.** (2018). A Damage Sensor Associated with the
591 Cuticle Coordinates Three Core Environmental Stress Responses in
592 *Caenorhabditis elegans*. *Genetics* **208**, 1467–1482.
593 **Eick, G. N. and Thornton, J. W.** (2011). Evolution of steroid receptors from an
594 estrogen-sensitive ancestral receptor. *Mol. Cell. Endocrinol.* **334**, 31–38.
595 **Fernandez, A. P., Gibbons, J. and Okkema, P. G.** (2004). *C. elegans peb-1* mutants
596 exhibit pleiotropic defects in molting, feeding, and morphology. *Dev. Biol.* **276**,
597 352–366.
598 **Fielenbach, N. and Antebi, A.** (2008). *C. elegans* dauer formation and the molecular
599 basis of plasticity. *Genes Dev.* **22**, 2149–2165.
600 **Forman-Rubinsky, R., Cohen, J. D. and Sundaram, M. V.** (2017). Lipocalins Are
601 Required for Apical Extracellular Matrix Organization and Remodeling in
602 Caenorhabditis elegans. *Genetics* **207**, 625–642.
603 **Frand, A. R., Russel, S. and Ruvkun, G.** (2005). Functional Genomic Analysis of *C.*

604 *elegans* Molting. *PLoS Biol.* **3**, e312.
605 **Gerisch, B. and Antebi, A.** (2004). Hormonal signals produced by DAF-9/cytochrome
606 P450 regulate *C. elegans* dauer diapause in response to environmental cues.
607 *Development* **131**, 1765–1776.
608 **Gerisch, B., Weitzel, C., Kober-Eisermann, C., Rottiers, V. and Antebi, A.** (2001). A
609 hormonal signaling pathway influencing *C. elegans* metabolism, reproductive
610 development, and life span. *Dev. Cell* **1**, 841–851.
611 **Ghedin, E., Wang, S., Spiro, D., Caler, E., Zhao, Q., Crabtree, J., Allen, J. E.,**
612 **Delcher, A. L., Guiliano, D. B., Miranda-Saavedra, D., et al.** (2007). Draft
613 genome of the filarial nematode parasite *Brugia malayi*. *Science* **317**, 1756–
614 1760.
615 **Gissendanner, C. R., Crossgrove, K., Kraus, K. A., Maina, C. V. and Sluder, A. E.**
616 (2004). Expression and function of conserved nuclear receptor genes in
617 *Caenorhabditis elegans*. *Dev. Biol.* **266**, 399–416.
618 **Goujon, M., McWilliam, H., Li, W., Valentin, F., Squizzato, S., Paern, J. and Lopez,**
619 **R.** (2010). A new bioinformatics analysis tools framework at EMBL–EBI. *Nucleic*
620 *Acids Res.* **38**, W695–W699.
621 **Gracida, X. and Eckmann, C. R.** (2013). Fertility and Germline Stem Cell Maintenance
622 under Different Diets Requires *nhr-114*/HNF4 in *C. elegans*. *Curr. Biol.* 1–7.
623 **Hao, L., Mukherjee, K., Liegeois, S., Baillie, D., Labouesse, M. and Bürglin, T. R.**
624 (2006). The hedgehog-related gene *qua-1* is required for molting in
625 *Caenorhabditis elegans*. *Dev. Dyn.* **235**, 1469–1481.
626 **Harfe, B. D., Gomes, A. V., Kenyon, C., Liu, J., Krause, M. and Fire, A.** (1998).
627 Analysis of a *Caenorhabditis elegans* Twist homolog identifies conserved and
628 divergent aspects of mesodermal patterning. *Genes Dev.* **12**, 2623–2635.
629 **Hauser, Y. P., Meeuse, M. W. M., Gaidatzis, D. and Großhans, H.** (2021). The BLMP-
630 1 transcription factor promotes oscillatory gene expression to achieve timely
631 molting. *bioRxiv* 2021.07.05.450828.
632 **Hendriks, G.-J., Gaidatzis, D., Aeschimann, F. and Großhans, H.** (2014). Extensive
633 oscillatory gene expression during *C. elegans* larval development. *Mol. Cell* **53**,
634 380–392.

635 **Huber, W., Carey, V. J., Gentleman, R., Anders, S., Carlson, M., Carvalho, B. S.,**
636 **Bravo, H. C., Davis, S., Gatto, L., Girke, T., et al.** (2015). Orchestrating high-
637 throughput genomic analysis with Bioconductor. *Nat. Methods* **12**, 115–121.
638 **Jetten, A. M.** (2009). Retinoid-related orphan receptors (RORs): critical roles in
639 development, immunity, circadian rhythm, and cellular metabolism. *Nucl. Recept.*
640 *Signal.* **7**,.
641 **Jumper, J., Evans, R., Pritzel, A., Green, T., Figurnov, M., Ronneberger, O.,**
642 **Tunyasuvunakool, K., Bates, R., Žídek, A., Potapenko, A., et al.** (2021).
643 Highly accurate protein structure prediction with AlphaFold. *Nature* **596**, 583–
644 589.
645 **Kage-Nakadai, E., Kobuna, H., Kimura, M., Gengyo-Ando, K., Inoue, T., Arai, H.**
646 **and Mitani, S.** (2010). Two very long chain fatty acid acyl-CoA synthetase
647 genes, *acs-20* and *acs-22*, have roles in the cuticle surface barrier in
648 *Caenorhabditis elegans*. *PLoS ONE* **5**, e8857.
649 **Kallen, J. A., Schlaeppi, J.-M., Bitsch, F., Geisse, S., Geiser, M., Delhon, I. and**
650 **Fournier, B.** (2002). X-Ray Structure of the hRORα LBD at 1.63 Å: Structural
651 and Functional Data that Cholesterol or a Cholesterol Derivative Is the Natural
652 Ligand of RORα. *Structure* **10**, 1697–1707.
653 **Kallen, J., Schlaeppi, J.-M., Bitsch, F., Delhon, I. and Fournier, B.** (2004). Crystal
654 structure of the human RORalpha Ligand binding domain in complex with
655 cholesterol sulfate at 2.2 A. *J. Biol. Chem.* **279**, 14033–14038.
656 **Kang, T.-H., Lindsey-Boltz, L. A., Reardon, J. T. and Sancar, A.** (2010). Circadian
657 control of XPA and excision repair of cisplatin-DNA damage by cryptochrome
658 and HERC2 ubiquitin ligase. *Proc. Natl. Acad. Sci.* **107**, 4890–4895.
659 **Kaplan, R. E. W. and Baugh, L. R.** (2016). L1 arrest, *daf-16*/FoxO and nonautonomous
660 control of post-embryonic development. *Worm* **5**, e1175196.
661 **Kasuga, H., Fukuyama, M., Kitazawa, A., Kontani, K. and Katada, T.** (2013). The
662 microRNA miR-235 couples blast-cell quiescence to the nutritional state. *Nature*
663 **497**, 503–506.
664 **Kelley, M., Yochem, J., Krieg, M., Calixto, A., Heiman, M. G., Kuzmanov, A., Meli,**
665 **V., Chalfie, M., Goodman, M. B., Shaham, S., et al.** (2015). FBN-1, a fibrillin-

666 related protein, is required for resistance of the epidermis to mechanical
667 deformation during *C. elegans* embryogenesis. *eLife* **4**, 1629.
668 **Kennaway, D. J., Boden, M. J. and Varcoe, T. J.** (2012). Circadian rhythms and
669 fertility. *Mol. Cell. Endocrinol.* **349**, 56–61.
670 **Kim, D. hyun, Grün, D. and van Oudenaarden, A.** (2013). Dampening of expression
671 oscillations by synchronous regulation of a microRNA and its target. *Nat. Genet.*
672 **45**, 1337–1344.
673 **King-Jones, K. and Thummel, C. S.** (2005). Nuclear receptors-a perspective from
674 Drosophila. *Nat. Rev. Genet.* **6**, 311–323.
675 **Kostrouchova, M., Krause, M., Kostrouch, Z. and Rall, J. E.** (1998). CHR3: a
676 *Caenorhabditis elegans* orphan nuclear hormone receptor required for proper
677 epidermal development and molting. *Development* **125**, 1617–1626.
678 **Kostrouchova, M., Krause, M., Kostrouch, Z. and Rall, J. E.** (2001). Nuclear
679 hormone receptor CHR3 is a critical regulator of all four larval molts of the
680 nematode *Caenorhabditis elegans*. *Proc. Natl. Acad. Sci. U. S. A.* **98**, 7360–
681 7365.
682 **Kouns, N. A., Nakielna, J., Behensky, F., Krause, M. W., Kostrouch, Z. and**
683 **Kostrouchova, M.** (2011). NHR-23 dependent collagen and hedgehog-related
684 genes required for molting. *Biochem. Biophys. Res. Commun.* **413**, 515–520.
685 **Kramer, J. M. and Johnson, J. J.** (1993). Analysis of mutations in the sqt-1 and rol-6
686 collagen genes of Caenorhabditis elegans. *Genetics* **135**, 1035–1045.
687 **Krasowski, M. D., Reschly, E. J. and Ekins, S.** (2008). INTRINSIC DISORDER IN
688 NUCLEAR HORMONE RECEPTORS. *J. Proteome Res.* **7**, 4359–4372.
689 **Lam, G. T., Jiang, C. and Thummel, C. S.** (1997). Coordination of larval and prepupal
690 gene expression by the DHR3 orphan receptor during Drosophila
691 metamorphosis. *Development* **124**, 1757–1769.
692 **Lažetić, V. and Fay, D. S.** (2017). Molting in *C. elegans*. *Worm* **6**, 1–20.
693 **Leng, X., Ding, T., Lin, H., Wang, Y., Hu, L., Hu, J., Feig, B., Zhang, W., Pusztai, L.,**
694 **Symmans, W. F., et al.** (2009). Inhibition of lipocalin 2 impairs breast
695 tumorigenesis and metastasis. *Cancer Res.* **69**, 8579–8584.
696 **Li, J., White, J. T., Saavedra, H., Wrabl, J. O., Motlagh, H. N., Liu, K., Sowers, J.,**

697 **Schroer, T. A., Thompson, E. B. and Hilser, V. J.** (2017). Genetically tunable
698 frustration controls allostery in an intrinsically disordered transcription factor.
699 *eLife* **6**, e30688.
700 **Lin, K., Dorman, J. B., Rodan, A. and Kenyon, C.** (1997). *daf-16*: An HNF-3/forkhead
701 family member that can function to double the life-span of *Caenorhabditis*
702 *elegans*. *Science* **278**, 1319–1322.
703 **Macneil, L. T., Watson, E., Arda, H. E., Zhu, L. J. and Walhout, A. J. M.** (2013). Diet-
704 Induced Developmental Acceleration Independent of TOR and Insulin in *C.*
705 *elegans*. *Cell* **153**, 240–252.
706 **Meeuse, M. W., Hauser, Y. P., Morales Moya, L. J., Hendriks, G., Eglinger, J.,**
707 **Bogaarts, G., Tsiairis, C. and Großhans, H.** (2020). Developmental function
708 and state transitions of a gene expression oscillator in *Caenorhabditis elegans*.
709 *Mol. Syst. Biol.* **16**,.
710 **Melo, J. A. and Ruvkun, G.** (2012). Inactivation of conserved C. elegans genes
711 engages pathogen- and xenobiotic-associated defenses. *Cell* **149**, 452–466.
712 **modENCODE Consortium, Roy, S., Ernst, J., Kharchenko, P. V., Kheradpour, P.,**
713 **Nègre, N., Eaton, M. L., Landolin, J. M., Bristow, C. A., Ma, L., et al.** (2010).
714 Identification of functional elements and regulatory circuits by Drosophila
715 modENCODE. *Science* **330**, 1787–1797.
716 **Mok, D. Z. L., Sternberg, P. W. and Inoue, T.** (2015). Morphologically defined sub-
717 stages of C. elegans vulval development in the fourth larval stage. *BMC Dev.*
718 *Biol.* 1–8.
719 **Morse, D., Cermakian, N., Brancorsini, S., Parvinen, M. and Sassone-Corsi, P.**
720 (2003). No circadian rhythms in testis: Period1 expression is clock independent
721 and developmentally regulated in the mouse. *Mol. Endocrinol.* **17**, 141–151.
722 **Mullaney, B. C., Blind, R. D., Lemieux, G. A., Perez, C. L., Elle, I. C., Faergeman, N.**
723 **J., Van Gilst, M. R., Ingraham, H. A. and Ashrafi, K.** (2010). Regulation of *C.*
724 *elegans* fat uptake and storage by acyl-CoA synthase-3 is dependent on NR5A
725 family nuclear hormone receptor *nhr-25*. *Cell Metab.* **12**, 398–410.
726 **Nelson, F. K., Albert, P. S. and Riddle, D. L.** (1983). Fine structure of the
727 *Caenorhabditis elegans secretory-excretory system*. *J. Ultrastruct. Res.* **82**, 156–

728 171.
729 **Page, A. P. and Johnstone, I. L.** (2007). The cuticle. *WormBook* 1–15.
730 **Patel, R. and Frand, A. R.** (2018). A Regulatory Loop between the Retinoid-Related
731 Orphan Nuclear Receptor NHR-23 and *let-7* family microRNAs Modulates the *C.*
732 *elegans* Molting Cycle. *bioRxiv* 1–47.
733 **Paus, R. and Foitzik, K.** (2004). In search of the "hair cycle clock": a guided tour.
734 *Differentiation* **72**, 489–511.
735 **Posch, A., Kohn, J., Oh, K., Hammond, M. and Liu, N.** (2013). V3 stain-free workflow
736 for a practical, convenient, and reliable total protein loading control in western
737 blotting. *J. Vis. Exp.* 50948.
738 **Pujol, N., Cypowyj, S., Ziegler, K., Millet, A., Astrain, A., Goncharov, A., Jin, Y.,**
739 **Chisholm, A. D. and Ewbank, J. J.** (2008). Distinct innate immune responses to
740 infection and wounding in the *C. elegans* epidermis. *Curr. Biol.* **18**, 481–489.
741 **R Core Team** *R: A language and environment for statistical computing.* Vienna,
742 Austria: R Foundation for Statistical Computing.
743 **Ragle, J. M., Aita, A. L., Morrison, K. N., Martinez-Mendez, R., Saeger, H. N.,**
744 **Ashley, G. A., Johnson, L. C., Schubert, K. A., Shakes, D. C. and Ward, J. D.**
745 (2020). The conserved molting/circadian rhythm regulator NHR-23/NR1F1 serves
746 as an essential co-regulator of *C. elegans* spermatogenesis. *Development* **147**,
747 dev193862.
748 **Roach, N. P., Sadowski, N., Alessi, A. F., Timp, W., Taylor, J. and Kim, J. K.** (2020).
749 The full-length transcriptome of *C. elegans* using direct RNA sequencing.
750 *Genome Res.*
751 **Ruaud, A.-F. and Bessereau, J.-L.** (2006). Activation of nicotinic receptors uncouples
752 a developmental timer from the molting timer in *C. elegans*. *Development* **133**,
753 2211–2222.
754 **Ruaud, A.-F., Lam, G. and Thummel, C. S.** (2010). The Drosophila nuclear receptors
755 DHR3 and FTZ-F1 control overlapping developmental responses in late
756 embryos. *Development* **137**, 123–131.
757 **Sandhu, A., Badal, D., Sheokand, R., Tyagi, S. and Singh, V.** (2021). Specific
758 collagens maintain the cuticle permeability barrier in *Caenorhabditis elegans*.

759 *Genetics* **217**,.
760 **Schindler, A. J., Baugh, L. R. and Sherwood, D. R.** (2014). Identification of Late
761 Larval Stage Developmental Checkpoints in *Caenorhabditis elegans* Regulated
762 by Insulin/IGF and Steroid Hormone Signaling Pathways. *PLoS Genet.* **10**,
763 e1004426.
764 **Sever, R. and Glass, C. K.** (2013). Signaling by Nuclear Receptors. *Cold Spring Harb.*
765 *Perspect. Biol.* **5**, a016709.
766 **Sievers, F., Wilm, A., Dineen, D., Gibson, T. J., Karplus, K., Li, W., Lopez, R.,**
767 **McWilliam, H., Remmert, M., Söding, J., et al.** (2011). Fast, scalable
768 generation of high-quality protein multiple sequence alignments using Clustal
769 Omega. *Mol. Syst. Biol.* **7**, 539.
770 **Simmons, C. A., Bledsoe, R. K., Guex, N. and Pearce, K. H.** (2008). Expression,
771 purification, and characterization of multiple, multifunctional human glucocorticoid
772 receptor proteins. *Protein Expr. Purif.* **62**, 29–35.
773 **Singh, R. N. and Sulston, J. E.** (1978). Some observations on molting in *C. elegans*.
774 *Nematologica* **24**, 63–71.
775 **Soroosh, P., Wu, J., Xue, X., Song, J., Sutton, S. W., Sablad, M., Yu, J., Nelen, M. I.,**
776 **Liu, X., Castro, G., et al.** (2014). Oxysterols are agonist ligands of RORγt and
777 drive Th17 cell differentiation. *Proc. Natl. Acad. Sci.* **111**, 12163–12168.
778 **Stec, N., Doerfel, K., Hills-Muckey, K., Ettorre, V. M., Ercan, S., Keil, W. and**
779 **Hammell, C. M.** (2021). An Epigenetic Priming Mechanism Mediated by Nutrient
780 Sensing Regulates Transcriptional Output during *C. elegans* Development. *Curr.*
781 *Biol.* **31**, 809-826.e6.
782 **Stempor, P. and Ahringer, J.** (2016). SeqPlots - Interactive software for exploratory
783 data analyses, pattern discovery and visualization in genomics. *Wellcome Open*
784 *Res.* **1**, 14.
785 **Sulston, J. E. and Horvitz, H. R.** (1977). Post-embryonic cell lineages of the
786 nematode, *Caenorhabditis elegans*. *Dev. Biol.* **56**, 110–156.
787 **Taubert, S., Ward, J. D. and Yamamoto, K. R.** (2011). Nuclear hormone receptors in
788 nematodes: Evolution and function. *Mol. Cell. Endocrinol.* **334**, 49–55.
789 **Telford, M. J., Bourlat, S. J., Economou, A., Papillon, D. and Rota-Stabelli, O.**

790 (2008). The evolution of the Ecdysozoa. *Philos. Trans. R. Soc. B Biol. Sci.* **363**,
791 1529–1537.
792 **Teuscher, A. C., Jongsma, E., Davis, M. N., Statzer, C., Gebauer, J. M., Naba, A.**
793 **and Ewald, C. Y.** (2019). The *in-silico* characterization of the *Caenorhabditis*
794 *elegans* matrisome and proposal of a novel collagen classification. *Matrix Biol.*
795 *Plus* **1**, 100001.
796 **Thummel, C. S.** (1990). Puffs and gene regulation-molecular insights into the
797 Drosophila ecdysone regulatory hierarchy. *BioEssays News Rev. Mol. Cell. Dev.*
798 *Biol.* **12**, 561–568.
799 **Tsiairis, C. and Großhans, H.** (2021). Chapter Two - Gene expression oscillations in
800 *C. elegans* underlie a new developmental clock. In *Current Topics in*
801 *Developmental Biology* (ed. Jarriault, S. and Podbilewicz, B.), pp. 19–43.
802 Academic Press.
803 **Van Gilst, M. R., Hadjivassiliou, H., Jolly, A. and Yamamoto, K. R.** (2005a). Nuclear
804 hormone receptor NHR-49 controls fat consumption and fatty acid composition in
805 *C. elegans*. *PLoS Biol.* **3**, e53.
806 **Van Gilst, M. R., Hadjivassiliou, H. and Yamamoto, K. R.** (2005b). A *Caenorhabditis*
807 *elegans* nutrient response system partially dependent on nuclear receptor NHR-
808 49. *Proc. Natl. Acad. Sci. U. S. A.* **102**, 13496–13501.
809 **Vo, A. A., Levenson, M. T., Ragle, J. M. and Ward, J. D.** (2021). Efficient generation
810 of a single-copy *eft-3p::TIR1::F2A:: BFP::AID*::NLS* allele in the *C. elegans*
811 *ttTi5605* insertion site through recombination-mediated cassette exchange.
812 *MicroPublication Biol.* **2021**, 10.17912/micropub.biology.000425
813 **Vogel, C. and Marcotte, E. M.** (2012). Insights into the regulation of protein abundance
814 from proteomic and transcriptomic analyses. *Nat. Rev. Genet.* **13**, 227–232.
815 **Vuong-Brender, T. T. K., Suman, S. K. and Labouesse, M.** (2017). The apical ECM
816 preserves embryonic integrity and distributes mechanical stress during
817 morphogenesis. *Development* **144**, 4336–4349.
818 **Ward, J. D.** (2015a). Rapid and Precise Engineering of the *Caenorhabditis elegans*
819 Genome with Lethal Mutation Co-Conversion and Inactivation of NHEJ Repair.
820 *Genetics* **199**, 363–377.

821 **Ward, J. D.** (2015b). Rendering the Intractable More Tractable: Tools from
822 *Caenorhabditis elegans* Ripe for Import into Parasitic Nematodes. *Genetics* **201**,
823 1279–1294.
824 **Ward, J. D., Bojanala, N., Bernal, T., Ashrafi, K., Asahina, M. and Yamamoto, K. R.**
825 (2013). Sumoylated NHR-25/NR5A Regulates Cell Fate during *C. elegans* Vulval
826 Development. *PLoS Genet.* **9**, e1003992.
827 **Ward, J. D., Mullaney, B., Schiller, B. J., He, L. D., Petnic, S. E., Couillault, C.,**
828 **Pujol, N., Bernal, T. U., Van Gilst, M. R., Ashrafi, K., et al.** (2014). Defects in
829 the *C. elegans* acyl-CoA Synthase, *acs-3*, and Nuclear Hormone Receptor, *nhr-*
830 *25*, Cause Sensitivity to Distinct, but Overlapping Stresses. *PLoS ONE* **9**,
831 e92552.
832 **Waterhouse, A. M., Procter, J. B., Martin, D. M. A., Clamp, M. and Barton, G. J.**
833 (2009). Jalview Version 2—a multiple sequence alignment editor and analysis
834 workbench. *Bioinformatics* **25**, 1189–1191.
835 **Yan, L., Borregaard, N., Kjeldsen, L. and Moses, M. A.** (2001). The high molecular
836 weight urinary matrix metalloproteinase (MMP) activity is a complex of gelatinase
837 B/MMP-9 and neutrophil gelatinase-associated lipocalin (NGAL). Modulation of
838 MMP-9 activity by NGAL. *J. Biol. Chem.* **276**, 37258–37265.
839 **Zaslaver, A., Mayo, A. E., Rosenberg, R., Bashkin, P., Sberro, H., Tsalyuk, M.,**
840 **Surette, M. G. and Alon, U.** (2004). Just-in-time transcription program in
841 metabolic pathways. *Nat. Genet.* **36**, 486–491.
842 **Zhang, L., Ward, J. D., Cheng, Z. and Dernburg, A. F.** (2015). The auxin-inducible
843 degradation (AID) system enables versatile conditional protein depletion in *C.*
844 *elegans*. *Development* **142**, 4374–4384.
845 **Zugasti, O., Rajan, J. and Kuwabara, P. E.** (2005). The function and expansion of the
846 Patched- and Hedgehog-related homologs in C. elegans. *Genome Res.* **15**,
847 1402–1410.
848

Materials and Methods

C. elegans Strains and Culture

C. elegans strains were cultured as originally described (Brenner, 1974), except worms were grown on MYOB instead of NGM. MYOB was made as previously described (Church et al., 1995). Animals were cultured at 20ºC for all assays, unless otherwise indicated. For general strain propagation, animals were grown at 15ºC according to standard protocols.

Strains used in this study

Strain	Genotype
JDW3	*nhr-23(wrd1[GFP^BioTag-degron-3xFLAG]) I; ; ieSi57 [Peft-3::TIR1::mRuby::unc-54 3'UTR, cb-unc-119(+)] II* (Ragle et al., 2020)
JDW230	*wrdSi40 [SCMp*:TIR1::F2A::mTagBFP2::AID*::NLS::tbb-2 +SEC II:0.77]* (Ashley et al., 2021)
JDW258	*wrdSi22 [eft-3p::TIR1::F2A::mTagBFP2::AID*::NLS::tbb-2 3'UTR+SEC, I:-5.32] ; nhr-23(kry61(nhr-23::AID*-TEV-3xFLAG)) I* (Ashley et al., 2021)
JDW290	*nhr-23(kry61(nhr-23::AID*-TEV-3xFLAG))I; re313 [col-10p::TIR1::F2A::mTagBFP2::AID*::NLS::tbb-2 3'UTR] II:0.77, II*
JDW291	*nhr-23(kry61(nhr-23::AID*-TEV-3xFLAG))I; reSi7 [rgef-1p::TIR1::F2A::mTagBFP2::AID*::NLS::tbb-2 3'UTR I:-5.32], I*
JDW292	*nhr-23(kry61(nhr-23::AID*-TEV-3xFLAG))I; ieSi61 [ges-1p::TIR1::mRuby::unc-54 3'UTR + Cbr-unc-119(+)] II.*
JDW294	*nhr-23(kry61(nhr-23::AID*-TEV-3xFLAG))I; cpSi171 [vha-8p::TIR1::F2A::BFP::AID*::NLS::tbb-2 3'UTR I:-5.32] I*
JDW310	*nhr-23(kry61(nhr-23::AID*-TEV-3xFLAG))I; wrdSi40 [SCMp*::TIR1::F2A::mTagBFP2::AID*::NLS::tbb-2 +SEC II:0.77]*

JDW311	*nhr-23(kry61(nhr-23::AID*-TEV-3xFLAG))I; wrdSi44 [SCMp*::TIR1::F2A::mTagBFP2::AID*::NLS::tbb-2 3'UTR, II:0.77 ttTi5605]*
JDW348	*ieSi57 [Peft-3::TIR1::mRuby::unc-54 3'UTR, cb-unc-119(+?)] II; frIs7 [nlp-29p::GFP + col-12p::DsRed] IV*
JDW349	*nhr-23(kry61(nhr-23::AID*-TEV-3xFLAG))I; ieSi57 [Peft-3::TIR1::mRuby::unc-54 3'UTR, cb-unc-119(+?)] II; frIs7 [nlp-29p::GFP +col-12p::DsRed] IV*
JDW350	*ieSi57 [Peft-3::TIR1::mRuby::unc-54 3'UTR, cb-unc-119(+?)] II; dhIs64 [daf-9p::daf-9::GFP + lin-15(+)]*
JDW351	*nhr-23(kry61(nhr-23::AID*-TEV-3xFLAG))I; ieSi57 [Peft-3::TIR1::mRuby::unc-54 3'UTR, cb-unc-119(+?)] II; dhIs64 [daf-9p::daf-9::GFP + lin-15(+)]*
JDW352	*ieSi57 [Peft-3::TIR1::mRuby::unc-54 3'UTR, cb-unc-119(+?)] II; ayIs6 [hlh-8::GFP fusion + dpy-20(+)] X*
JDW353	*nhr-23(kry61(nhr-23::AID*-TEV-3xFLAG))I; ieSi57 [Peft-3::TIR1::mRuby::unc-54 3'UTR, cb-unc-119(+?)] II; ayIs6 [hlh-8::GFP fusion + dpy-20(+)] X*
JDW354	*wrdSi60 [eft-3p::TIR1::F2A::mTagBFP2::AID*::NLS::tbb-2:tbb-2 3'UTR, I:-5.32] I; ayIs6 [hlh-8::GFP fusion + dpy-20(+)] X*
JDW355	*wrdSi61 [eft-3p::TIR1::F2A::mTagBFP2::AID*::NLS::tbb-2:tbb-2 3'UTR, I:-5.32] ; nhr-23(kry61(nhr-23::AID*-TEV-3xFLAG)) I; ayIs6 [hlh-8::GFP fusion + dpy-20(+)] X*
JDW356	*wrdSi59 [eft-3p::TIR1::F2A::mTagBFP2::AID*::NLS::tbb-2 3'UTR, I:-5.32], daf-16(mu86) I; ayIs6 [hlh-8::GFP fusion + dpy-20(+)] X*
JDW357	*wrdSi59 [eft-3p::TIR1::F2A::mTagBFP2::AID*::NLS::tbb-2 3'UTR, I:-5.32], nhr-23(kry61(nhr-23::AID*-TEV-3xFLAG)), daf-16(mu86) I; ayIs6 [hlh-8::GFP fusion + dpy-20(+)] X*

858

KRY87	*nhr-23(kry61(nhr-23::AID*-TEV-3xFLAG))I* (Zhang et al., 2015)
KRY88	*nhr-23(kry61(nhr-23::AID*-TEV-3xFLAG))I; ieSi57 [Peft-3::TIR1::mRuby::unc-54 3'UTR, cb-unc-119(+?)] II* (Zhang et al., 2015)

Strains provided by the CGC

Strain	Genotype
AA277	*lin-15B&lin-15A(n765) X; dhIs64 [daf-9p::daf-9::GFP + lin-15(+)]* (Gerisch and Antebi, 2004)
PD4666	*ayIs6 [hlh-8::GFP fusion + dpy-20(+)] X* (Harfe et al., 1998)
CA1200	*unc-119(ed3); ieSi57 [Peft-3::TIR1::mRuby::unc-54 3'UTR, cb-unc-119(+)] II* (Zhang et al., 2015)
CA1209	*ieSi61 [ges-1p::TIR1::mRuby::unc-54 3'UTR + Cbr-unc-119(+)] II*
CF1038	*daf-16(mu86) I* (Lin et al., 1997)
DV3800	*reSi2 [col-10p::TIR1::F2A::mTagBFP2::AID*::NLS::tbb-2 3'UTR II:0.77]* (Ashley et al., 2021)
DV3805	*reSi7 [rgef-1p::TIR1::F2A::mTagBFP2::AID*::NLS::tbb-2 3'UTR I:-5.32]* (Ashley et al., 2021)
JDW118	*wrdSi22 [eft-3p:TIR1:F2A:mTagBFP2:tbb-2 3'UTR+SEC, I:-5.32] (Vo et al., 2021)*
JDW224	*wrdSi22 [eft-3p::TIR1::F2A::mTagBFP2::AID*::NLS::tbb-2 3'UTR+SEC, I:-5.32]* (Ashley et al., 2021)
LP869	*cpSi171 [vha-8p::TIR1::F2A::mTagBFP::AID*::NLS::tbb-2 3'UTR I:-5.32]* (Ashley et al., 2021)

864

865 **Auxin treatment**

866 Control and auxin media/plates were made as described in Ragle et al. 2020. Control
867 media consisted of MYOB agar+0.25% ethanol. Auxin media was made by dissolving
868 indole 3-acetic acid (Alfa Aesar, AAA1055622) in 100% ethanol to 1.6 M and then mixing
869 it into melted MYOB agar at 55°C to a final concentration of 4 mM prior to pouring plates.
870 Temperature of the media was monitored with a Lasergrip 1080 infrared thermometer gun
871 (Etekcity). Plates were seeded with *E. coli* OP50 and incubated overnight at room
872 temperature. Plates were stored for up to one month at 4ºC prior to use. For all auxin
873 treatment experiments, animals were synchronized by alkaline bleaching. The collected
874 eggs were incubated in M9 buffer supplemented with 5mg/mLcholesterol at 20ºC for 24
875 hours and arrested L1 larvae were released onto the indicated type of MYOB plate.

876

877 **Microscopy**

878 Synchronized animals were collected from MYOB, control, or auxin plates at the indicated
879 time points using 1000µl of M9 + 2% gelatin. Animals were spun at 700xg for 1 min. The
880 media was then aspirated off and animals were resuspended in 500µl M9 + 2% gelatin
881 with 5 mM levamisole. 12µl of animals in M9 +gel with levamisole solution were placed
882 on slides with a 2% agarose pad and secured with a coverslip. Images were acquired
883 using a Plan-Apochromat 40x/1.3 Oil DIC lens on an AxioImager M2 microscope (Carl
884 Zeiss Microscopy, LLC) equipped with a Colibri 7 LED light source and an Axiocam 506
885 mono camera. Acquired images were processed through Fiji software (version: 2.0.0- rc-
886 69/1.52p). For direct comparisons within a figure, we set the exposure conditions to avoid
887 pixel saturation of the brightest sample and kept equivalent exposure for imaging of the
888 other samples.

889

890 **Phenotypic analysis**

891 For the phenotypic analysis in Figure 2, synchronized CA1200 or KRY88 larvae were
892 released onto MYOB plates and then shifted onto control or auxin plates every two hours
893 up to 16 hours. Animals were collected as described in the Microscopy section and
894 imaged by DIC microscopy to score for morphology and shedding of the L1 cuticles. For

895 the M cell lineage experiments in Figures 4C and 5A, synchronized animals of the
896 indicated genotypes were released onto MYOB plates and shifted onto control or auxin
897 plates at 3 hours (early shift) or 9 hours (late shift) post-release and then imaged at 24
898 hours post-release, as described in the Microscopy section. M cells were counted and
899 recorded. For the L3 shift experiments (Fig. 4D,5B) synchronized animals of the indicated
900 genotype were grown on MYOB. At 25 hours post-release, they were shifted onto 6-well
901 control or auxin MYOB plates seeded with OP50. 24 hours later, animals were collected
902 as described in the Microscopy section and imaged by DIC microscopy to stage animals
903 according to vulval morphology (Mok et al., 2015).
904
905 **Hypo-osmotic stress sensitivity**
906 Hypo-osmotic stress sensitivity assays were performed on L4 stage larvae as described
907 (Ward et al., 2014), except we used 20µl of dH_20. Each strain was assayed in triplicate.
908
909 **Western Blots**
910 Animals were synchronized by alkaline bleaching, as described in the Auxin Treatment
911 section. For the western blots in Figure 1C and 2B, 6000 KRY88 animals per well were
912 transferred onto a 6-well MYOB plate seeded with OP50. Animals were cultured at 20ºC
913 and collected at the indicated timepoints as previously described by washing animals out
914 of the well with M9+0.05% gelatin (VWR, 97062-620), transferring to a 1.5 ml tube and
915 washing twice more with M9+0.05% gelatin (Vo et al., 2021). Animals were pelleted,
916 transferred in a 30 µl volume to a new 1.5 ml tube, and flash frozen in liquid nitrogen. For
917 the western blot in Figure 2B, synchronized KRY87 animals were grown at 20ºC on
918 MYOB plates, before being washed off in M9+0.05% gelatin. A 0 minute time point was
919 collected as described above, and then 6000 animals were transferred into the wells of a
920 6-well control or auxin plate seeded with OP50. Samples were collected at 15 and 30
921 minutes following transfer into the well, as described above. For the western blots in
922 Figure 3B, 500 animals of the indicated genotype were transferred into wells of a 6-well
923 control or auxin plate seeded with OP50. Animals were incubated for 24 hours at 20ºC
924 and collected as described above. To generate the lysate for western blot analysis,
925 animals were freeze-cracked twice in liquid nitrogen, and Laemmli sample buffer was

926 added to 1X and samples were heated to 95ºC for 10 minutes. The resulting supernatants
927 were used for western blot analysis, as described below.
928
929 For the blots in Figures 1C and 2B 10 µl of lysate and 7.5 µl 1:1 mix of Amersham ECL
930 Rainbow Molecular Weight Markers (95040-114) and Precision Plus Protein Unstained
931 Standards (1610363) was resolved by SDS-PAGE using precast 4-20% MiniProtean TGX
932 Stain Free Gels (Bio-Rad). For the blot in Figure 3B, the lysates had more variable levels
933 of total protein, particularly the NHR-23 depleted samples that produced an early larval
934 arrest. Therefore we quantified the signal of the most intense band by Stain Free imaging
935 (Posch et al., 2013) using a Bio-Rad ChemiDoc imaging system, and ran a new gel with
936 normalized loading. Proteins were transferred to a polyvinylidene difluoride membrane by
937 semi-dry transfer with a TransBlot Turbo (Bio-Rad). Total protein, pre- and post-transfer,
938 was monitored using the stain-free fluorophore as described (Posch et al., 2013; Ward,
939 2015a). Membranes were washed in TBST and blocked in TBST+5% milk (TBST-M;
940 Nestle Carnation Instant Nonfat Dry Milk, 25.6-Ounce, Amazon) for one hour at room
941 temperature. Blots were rocked in primary antibodies in TBST-M overnight at 4ºC and
942 then washed 4x5min with TBST. For primary antibodies conjugated with horseradish
943 peroxidase (HRP) the blots were developed after the last TBST wash. Otherwise, blots
944 were incubated with HRP-conjugated secondary antibodies in TBST-M for one hour at
945 room temperature followed by 4x5min TBST washes and then developed as described
946 below.
947
948 The primary antibody used for Figure 1C and 2B was horseradish peroxidase (HRP)
949 conjugated anti-FLAG M2 (Sigma-Aldrich, A8592-5x1MG, Lot #SLCB9703) at a 1:2000
950 dilution. Precision Protein StrepTactin-HRP Conjugate (Bio-Rad, #1610381, Lot
951 #64426657) was included with the primary antibody at a 1:10,000 dilution to visualize the
952 protein size standard during blot imaging. For the blot in Figure 3B, we used the following
953 1º antibodies diluted at 1:2000: rabbit anti-GFP antibody (Sigma Millipore, C1544-100µg)
954 and mouse anti-alpha-Tubulin 12G10 (Developmental Studies Hybridoma Bank, we used
955 the "-c" concentrated supernatant). The secondary antibodies were Digital anti-Rabbit
956 (Kindle Biosciences LLC, R1006) and Digital anti-mouse (Kindle Biosciences LLC,

957 R1005), both diluted 1:1000. Streptactin-HRP was included at 1:1000 with the 2º antibody
958 incubations, similar to the anti-FLAG M2-HRP blots. Blots were incubated for 5 minutes
959 with 1 ml of Supersignal West Femto Maximum Sensitivity Substrate (Thermo Fisher
960 Scientific, 34095) and the final blot were imaged using the 'chemi high-resolution' setting
961 on a Bio-Rad ChemiDoc MP System.
962
963 **Bioinformatics**
964 Figure 6A was generated in R (R Core Team). Phase and amplitude in Table S1 were
965 converted to x and y coordinates for each gene by calculating x = amplitude * cos(phase)
966 and y = amplitude * sin(phase). For Figure 6B and S6, L3 NHR-23 ChIP-Seq data was
967 downloaded from http://www.modencode.org, accession ID modEncode_3837. Wig files
968 were converted to bigwig format and loaded into the Bioconductor package SeqPlots
969 (cite_SeqPlots)(Huber et al., 2015; Stempor and Ahringer, 2016). A bed file with the start
970 and end coordinates of all genes' CDS was generated and loaded into SeqPlots. SeqPlots
971 aligned all genes by the start and end position and scaled the coding sequence of each
972 gene to 2 kb. The average signal over all aligned genes was calculated in 25 bp windows
973 from 1 kb upstream of the start site to 1kb downstream of the end site. For Fig. 6C the
974 phase for the oscillating genes in Table S1 was converted to time during the molting cycle
975 by assuming a 9 hour larval stage which make each hour=40º. The phase in hours was
976 then plotted along the x axis and the oscillating genes' amplitude was plotted on the y
977 axis. The gene annotation was based on the Concise Description and Automated
978 Description downloaded from Wormbase.
979
980 **Statistical Analysis**
981 Statistical tests and numbers of animals analyzed are detailed in figure legends.
982
983 **Competing interests**
984 The authors declare no competing or financial interests.
985
986
987

Acknowledgements

We thank Chris Hammell, David Matus, and Julian Ceron Madrigal for their critical reading of the manuscript. We thank Miles Pufall, Helge Grosshans, and Ali Shariati for helpful discussions. Some strains were provided by the *Caenorhabditis Genetics* Center, which is funded by the NIH Office of Research Infrastructure Programs.

Funding

This work was funded by the National Institutes of Health (NIH) National Institute of General Medical Sciences (NIGMS) [R01 GM138701] to J.D.W. Some strains were provided by the Caenorhabditis Genetics Center, which is funded by the NIH Office of Research Infrastructure Programs [P40 OD010440]. L.C.J. was funded by NIGMS training grants [T32 GM133391 and IMSD T32 GM135742]. J.A. was supported by an NIGMS grant supporting the MARC U*STAR program at UCSC [T34 GM007910]. The anti-alpha tubulin 12G10 monoclonal antibody developed by J. Frankel and E.M. Nelson of the University of Iowa was obtained from the Developmental Studies Hybridoma Bank, created by the NICHD of the NIH and maintained at The University of Iowa, Department of Biology, Iowa City, IA 52242.